A Machine Learning Approach to Resolving Conflicts in Physical Human-Robot Interaction

by

Enes Ulaş Dinçer

A Dissertation Submitted to the
Graduate School of Sciences and Engineering
in Partial Fulfillment of the Requirements for
the Degree of

Master of Science

in

Mechanical Engineering

KOÇ ÜNİVERSİTESİ

November 21, 2024

A Machine Learning Approach to Resolving Conflicts in Physical Human-Robot Interaction

Koç University
Graduate School of Sciences and Engineering

This is to certify that I have examined this copy of a master's thesis by

Enes Ulaş Dinçer

and have found that it is complete and satisfactory in all respects,
and that any and all revisions required by the final
examining committee have been made.

Committee Members:

____
Prof. Dr. Çağatay Basdoğan (Advisor)

____
Assoc. Prof. Aykut Erdem

____
Asst. Prof. Yusuf Aydın

Date: ______________________________

I dedicate this work to my loving family, who have been my constant source of support and encouragement throughout my academic journey. Your unwavering faith in me has been my greatest strength. To my girlfriend, Gamze Nur Yapıcı, whose patience, understanding, and support have been invaluable. Your presence in my life has made this journey more meaningful and worthwhile. To my friends, who have been there through both challenges and celebrations, providing much-needed laughter, support, and perspective along the way. Your friendship has made this journey not just bearable, but enjoyable. And to Prof. Dr. Çağatay Başdoğan, whose mentorship and guidance have shaped not only this work but also my academic path. Your expertise and dedication to excellence have been truly inspiring.

ABSTRACT

A Machine Learning Approach to Resolving Conflicts in Physical Human-Robot Interaction
Enes Ulaş Dinçer
Master of Science in Mechanical Engineering
November 21, 2024

As artificial intelligence techniques become more sophisticated, we anticipate that robots collaborating with humans will develop their own intentions, leading to potential conflicts in interaction. This development calls for advanced conflict resolution strategies in physical human-robot interaction (pHRI), a key focus of our research. We use a Machine Learning (ML) classifier to detect conflicts during co-manipulation tasks to adapt the robot's behavior accordingly using an admittance controller. In our approach, we focus on two groups of interactions, namely "harmonious" and "conflicting", corresponding to the cases of the human and the robot working in harmony to transport an object when they aim for the same target and human and robot are in conflict when human changes the manipulation plan such as a change in the direction of movement or parking location of the object, respectively.

Co-manipulation scenarios were designed to investigate the efficacy of the proposed ML approach, involving 20 participants. Task performance achieved by the ML approach was compared against three alternative approaches: a) a Rule-Based (RB) Approach, where interaction behaviors were rule-derived from statistical distributions of haptic features; b) an unyielding robot that is proactive during harmonious interactions but does not resolve conflicts otherwise, and c) a passive robot which always follows the human partner. This mode of cooperation is known as "hand guidance" in pHRI literature and is frequently used in industrial settings for so-called "teaching" a trajectory to a collaborative robot.

The results show that the proposed ML approach is superior to the others in task performance. However, a detailed questionnaire administered after the experiments, which contains several metrics, covering a spectrum of dimensions, to measure the subjective opinion of the participants reveals that the most preferred mode of interaction with the robot is surprisingly passive. This preference indicates a strong

inclination towards an interaction mode that gives more control to humans and offers less demanding interaction, even if it is not the most efficient in task performance. Hence, there is a clear trade-off between task performance and the preferred mode of interaction of humans with a robot, and a well-balanced approach is necessary for designing effective pHRI systems in the future.

ÖZETÇE

Fiziksel İnsan-Robot Etkileşiminde Çatışmaların Çözümü İçin Bir Makine Öğrenmesi Yaklaşımı
Enes Ulaş Dinçer
Makine Mühendisliği, Yüksek Lisans
November 21, 2024

Yapay zeka teknikleri ileride daha sofistike hale geldikçe, insanlarla işbirliği yapan robotların kendi niyetlerini geliştireceğini ve bu da insan-robot etkileşiminde potansiyel çatışmalara yol açacağını öngörüyoruz. Bu olası gelişme, fiziksel insan-robot etkileşimi alanında ileri düzey çatışma çözümleme stratejileri gerektirir ki bu da araştırmamızın temel odak noktasıdır. Bu tezde önerdiğimiz yaklaşımda, bir makine öğrenimi (MÖ) sınıflandırıcısı kullanarak işbirlikli manipülasyon görevleri sırasında çatışmaları tespit ediyor ve bir admitans kontrolcüsü kullanarak robotun davranışını buna göre uyarlıyoruz. İki grup etkileşime odaklanıyoruz, bunlar "uyumlu" ve "çatışmalı" olarak sınıflandırılmıştır. Bu sınıflar, sırasıyla insan ve robotun aynı hedef için birlikte bir nesneyi taşırken uyum içinde çalıştığı ve insanın manipülasyon planını, örneğin nesnenin hareket yönünü veya park yerini değiştirdiği zaman çatışma yaşandığı durumlara karşılık gelmektedir.

Önerilen MÖ yaklaşımının etkinliğini araştırmak için 20 deneğin katıldığı işbirlikli manipülasyon deneyleri tasarlandı. MÖ yaklaşımını kullanan robot ile elde edilen görev performansı, üç alternatif yaklaşımla elde edilen performanslarla karşılaştırıldı: a) Kural Tabanlı (KT) bir yaklaşım kullanan robot: bu yaklaşımda, etkileşimleri sınıflandırmak için haptik verilerin istatistiksel dağılımlarından yola çıkarak kurallar türetilmiştir; b) uyumlu etkileşimler sırasında proaktif olan ancak diğer durumlarda çatışmaları çözümleyemeyen dirençli bir robot; ve c) her zaman insanın komutlarını takip eden pasif bir robot. Bu son yaklaşım, fiziksel insan-robot etkileşimi literatüründe "el rehberliği" olarak bilinir ve endüstriyel ortamlarda işbirlikçi bir robota bir yörünge "öğretmek" için sıklıkla kullanılır.

Sonuçlar, önerilen MÖ yaklaşımının görev performansı açısından diğerlerinden üstün olduğunu göstermektedir. Ancak, deneylerden sonra uygulanan detaylı bir anket, robotun pasif olduğu yaklaşımın, süpriz şekilde, denekler tarafından en çok

tercih edildiğini göstermiştir. Bu seçim, görev performansı açısından verimli bir yaklaşım olmasa bile, insanlara daha fazla kontrol sağladığı ve daha az talepkar olduğu için tercih edilmiştir. Sonuç olarak bu tez, gelecekte etkili fiziksel insan-robot etkileşimi sistemleri geliştirmek için ortak görev performansı ile insanın subjektif etkileşim tercihleri arasında dengeli bir yaklaşım gerektiğini göstermektedir.

ACKNOWLEDGMENTS

First and foremost, I would like to express my deepest gratitude to my advisor, Prof. Dr. Çağatay Başdoğan, for his exceptional guidance, expertise, and support throughout this research. His insightful feedback and continuous encouragement have been instrumental in bringing this work to fruition. His dedication to research excellence and his ability to inspire students have profoundly influenced my academic development.

I would also like to extend my sincere thanks to Feras Kiki for his valuable collaboration and support during this research. His technical insights and constructive feedback have significantly contributed to the quality of this work.

I am grateful to my friends and colleagues who have supported me throughout this journey. Their academic insights, moral support, and friendship have made this experience both enriching and memorable. The countless discussions, both academic and personal, have contributed immensely to my growth during this period.

From the depths of my heart, thank you.

TABLE OF CONTENTS

LIST OF TABLES

LIST OF FIGURES

ABBREVIATIONS

ANN	Artificial Neural Network
APF	Artificial Potential Field
CD	Conflict in Target Direction
CP	Conflict in Parking Location
ELM	Extreme Learning Machine
EMG	Electromyography
IMU	Inertial Measurement Unit
LSTM	Long Short-Term Memory
ML	Machine Learning
pHRI	physical Human-Robot Interaction
RBF	Radial Basis Function
RB	Rule-Based
SVM	Support Vector Machine
WH	Working in Harmony

Chapter 1

INTRODUCTION

Recent advancements in robotics have revolutionized numerous industries, extending their applications to a wide range of tasks previously considered exclusive to human capabilities. As a result, physical human-robot interaction (pHRI) has emerged as a critical field of study, exploring the seamless integration of robots into human-centric environments, and fostering physical collaboration in shared workspaces. Collaborative object manipulation (co-manipulation), a fundamental aspect of pHRI, entails a human and a robot working in tandem to handle and transport an object.

In the near future, humans and robots are expected to perform co-manipulation tasks in various environments, such as homes (e.g. moving bulky furniture), hospitals (e.g. transporting a patient bed in corridors), and factories (e.g. assembling the windshield of a car). However, effective performance of such tasks requires good coordination between partners, supported by advanced resolution strategies to manage conflicts inherent to human physical interaction capabilities that robots have yet to achieve. The current challenge in co-manipulation is the need for a robust and adaptive control system to manage the physical interactions between the human and the robot, as well as advanced machine intelligence to comprehend and respond to the dynamic interaction patterns of human-robot collaboration. Without addressing these issues, co-manipulation tasks may result in inefficient performance, potential safety hazards, and a failure to fully leverage the capabilities of human-robot teams.

As a first step toward addressing this challenge, we design and implement a pHRI system geared toward facilitating co-manipulation between a human and a robot through conflict detection and resolution under scenarios encompassing both harmonious and conflicting interactions (see Figure 1.1). Specifically, we focus on the dyadic nature of interaction, going beyond the operation of single actors. In this paper, we present an experimental study where conflicting and harmonious scenarios are distinguished through three dyadic interaction patterns: Working in Harmony (WH), Conflict in Target Direction (CD), and Conflict in Parking Location (CP). WH represents a synergistic collaboration, while CD and CP involve discrepancies in movement direction or parking location, respectively. An ML method, as outlined in [Al-Saadi et al., 2023], is implemented to classify these distinct patterns. In our ML approach, we utilize haptic features extracted from the human and robot wrench data to train a Random Forest classifier. Based on the classified pattern, the robot adjusts its behavior accordingly: It can either proactively assist the human in object manipulation or passively follow the human's lead. We compare the performance of our ML-based robot with three robot behavior models: 1) an RB model that detects the interaction patterns based on pre-defined rules and accommodates the human

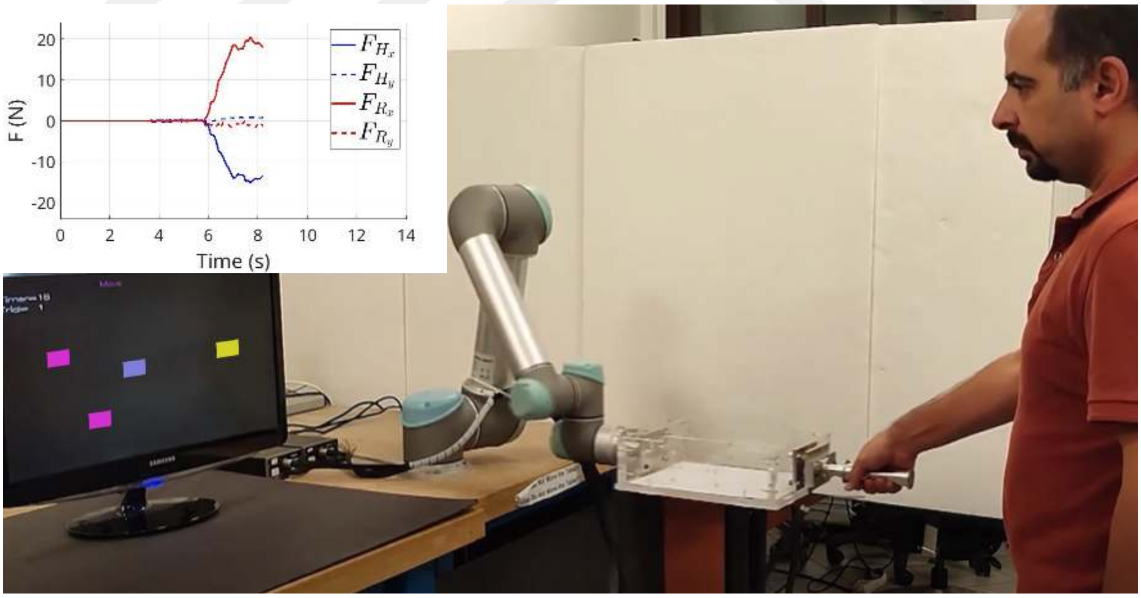

Figure 1.1: A scene from our human-robot co-manipulation experiments: a user engages with a collaborative robot to manipulate an object. The forces applied to the object by the user and the robot are measured by two separate force sensors in real-time as shown in the inline plot on the upper left corner. Note that the measured data were not displayed to the participants during the experiments but monitored by the experimenter to detect any potential issues during the experimentation.

partner to resolve the conflict (as is done in the ML-based model), 2) an unyielding robot that follows its own agenda with no conflict detection and resolution without accommodating the human, and 3) a passive robot that always follows the human (i.e. hand guidance).

Our goals in this paper are threefold: 1) to emphasize the importance of haptic information in detecting and resolving conflicts, 2) to validate the necessity of employing an ML approach through baseline comparison, and 3) develop an understanding of human perceptions of an autonomous robotic helper using the proposed ML approach. In this paper, we highlight the prevalence of haptics in co-manipulation and stress the importance of analyzing interactive elements through forces to accurately classify interaction patterns, rather than solely relying on human intent or behavior –as is often done in the literature. As artificial intelligence techniques become more sophisticated, we anticipate that robots collaborating with humans will develop their own intentions, leading to potential conflicts in interaction. This calls for advanced conflict resolution strategies in pHRI, a key focus of our research. In our recent work [Al-Saadi et al., 2023], we transferred the knowledge gained from human dyads to human-robot dyads, underscoring the importance of conflict identification and resolution as essential skills for robots in co-manipulation tasks. We utilized an ML model, trained with haptic data from human dyads, to classify the dyadic interaction patterns of human-robot dyads. We showed that this approach improves the task performance. In this study, we hypothesize that pHRI system design should go beyond optimizing task performance to also prioritize addressing human needs and preferences in physical interactions. In this regard, we extend our earlier work [Al-Saadi et al., 2023] through the following avenues:

- **Baseline comparison:** To justify the selection of our ML classifier (Random Forest), we first compared its performance with two other classifiers (ANN and SVM) using the training dataset. We then developed an RB approach for baseline comparison with our ML approach. A new testing experiment was designed and conducted to compare the performance of the proposed ML approach with the new RB approach. This new experiment involved manipulation scenarios containing a richer set of dyadic interaction patterns compared to our earlier work [Al-Saadi et al., 2023]. In this study, we also implemented an adaptive admittance controller to demonstrate the benefits of accurately detecting interaction patterns from a task performance perspective.

- **Subjective analysis of participants' perceptions:** To capture the personal opinions of the participants about the proposed pHRI system, we designed a questionnaire and administered it after the experiments. The questionnaire encompassed a broad spectrum of subjective experiences, including six questions of the NASA Task Load Index (TLX), measuring Mental Demand, Physical Demand, Temporal Demand, Performance, Effort, and Frustration. Beyond these workload-related questions, the questionnaire included 13 additional metrics to explore concepts crucial to human-robot interaction: Comfort, Trust, Enjoyment, Safety, Reliability, Responsiveness, Proactivity, Level of Control, Fluency, Robotic Assistance, Ease of Use, Perceived Usefulness, and Overall Satisfaction. These additional questions were formulated by us, leveraging our prior experiences in designing questionnaires for studies on human-robot interaction [Basdogan et al., 2000, Kucukyilmaz et al., 2013].

We conducted a series of experiments, using the four interaction modes: *ML*, *RB*, *Unyielding*, and *Passive*, as briefly mentioned above. Quantitative metrics, such as average force applied by the human, object velocity, and task completion time, are analyzed alongside subjective feedback from participants. The results show that the proposed pHRI system utilizing the ML model is superior to the others in task performance: it can successfully classify interaction patterns to adapt the robot's behavior, fostering a more efficient collaboration. However, surprisingly, participants favored the *Passive* mode for interactions with the robot based on the results of a questionnaire administered after the experiments.

This paper is organized as follows: Section 2 reviews relevant literature on pHRI. Section 3 outlines the methodology used to classify the dyadic interaction patterns and how the robot's behavior is adapted accordingly. Section 4 details the co-manipulation experiments conducted. Section 5 and Section 6 synthesizes the findings, and Section 7 concludes the paper, providing insights into potential future directions in this exciting research domain.

Chapter 2

RELATED WORK

2.1 Interaction Control for pHRI

In the context of pHRI, admittance and impedance controllers are frequently used to regulate the interaction between a human and a robot. An impedance controller receives input from the human in the form of position/velocity and produces a reference force to be tracked by the robot. On the other hand, an admittance controller aims to regulate the robot's position or velocity based on the force applied by the human. Impedance control allows for more precise control of the robot's motion, making it suitable for applications where accuracy and precision in movement are crucial while admittance control allows the robot to naturally respond to the forces exerted by the human user, as utilized in our earlier studies [Aydin et al., 2021, Aydin et al., 2020].

2.2 Adaptive Interaction Control for pHRI

To accommodate changing human intentions, earlier studies have focused on developing adaptive (variable) interaction (impedance/admittance) controllers. An adaptive interaction controller in the realm of pHRI offers distinct advantages over a standard interaction controller. This adaptability becomes particularly crucial in scenarios where human intentions change during the task [Losey et al., 2018, Hoffman et al., 2024]. The adaptive nature of these controllers, whether impedance or admittance, not only improves the task performance but also fosters a more natural and intuitive collaboration between humans and robots. The adaptation is typically achieved by changing the parameters of the interaction controller in real-time based on human intention. We consider two categories of algorithms that can be used to facilitate the adaptation process: RB and ML-based.

2.3 Rule-Based Approaches for Human Intent Detection

In approaches guided by rules, a predefined set of rules is established, typically relying on some thresholds related to kinematic or kinetic interaction variables to discern human movement intentions. Earlier studies have employed various combinations of object velocity, human force, and their derivatives [Wojtara et al., 2009, Kang et al., 2019, Lecours et al., 2012, Hamad et al., 2021] to anticipate human intentions, thereby adapting the parameters of an interaction controller of the robot during collaborative manipulation tasks. RB adaptation of an admittance controller based on the distance to the target was applied to collaborative drilling on flat [Sirintuna et al., 2020a] and also the more challenging case of curved surfaces [Madani et al., 2022]. The real-time adaptation of the admittance damping in these scenarios provides more transparency (minimal resistance to human movement) when driving the robot in free space to the target while ensuring stability during drilling at the target. RB methodologies have also been extended to handle situations involving role exchanges, aiming to discern human intentions in assuming either the leader or follower role. Oguz et al. [Oguz et al., 2010, Oguz et al., 2012] and Kucukyilmaz et al. [Kucukyilmaz et al., 2013] introduced mechanisms for dynamic role exchanges between humans and robots in collaborative haptic interaction tasks, inferring human intentions from forces applied to the manipulated object to adjust the robot's role. Subsequently, Mörtl et al. [Mörtl et al., 2012] expanded on these methods, formulating an RB strategy enabling dynamic role exchanges and task contribution adjustments between robot and human partners based on forces observed in a table co-manipulation task. Khoramshahi and Billard [Khoramshahi and Billard, 2019, Khoramshahi and Billard, 2020] proposed dynamical system approaches in pHRI, utilizing human-intended motion velocity to facilitate role-switching between a stiff leader and a compliant follower. The research by Bussy et al. [Bussy et al., 2012] showcases the proactive role adaptation of humanoid robots in pHRI. Their study on a humanoid robot in a haptic task demonstrates role-switching capabilities, underlining the adaptability and efficiency of robots in collaborative scenarios.

One disadvantage of an RB approach compared to an ML-based one in detecting human intention during pHRI is its reliance on explicitly defined rules. In an RB system, human experts need to formulate predetermined rules based on their understanding of the task and the interaction variables. These rules might capture known patterns or criteria for detecting specific intentions, but they may struggle to account for the complexity and variability inherent in human behavior. Moreover, crafting exhaustive rules to cover all possible scenarios and adapting them to the interaction context can be challenging.

2.4 Machine Learning Approaches for Human Intent Detection

In contrast, ML algorithms can learn complex patterns and relationships directly from data. They can adapt and generalize to diverse and evolving scenarios, potentially outperforming RB systems in situations with intricate, non-linear, or ambiguous patterns of human intention. As such, ML algorithms have been utilized for different purposes to increase adaptation capabilities in pHRI. Mielke et al. [Mielke et al., 2024] developed a deep neural network to predict human intent from motion data in human-human dyads, improving human-robot co-manipulation by distinguishing between rotational and translational movements. Townsend et al. [Townsend et al., 2017] employed an Artificial Neural Network (ANN) to predict future human velocity based on past velocity and acceleration, specifically in a human-human co-manipulation task. Cacace et al. [Cacace et al., 2018] utilized a 3-layer ANN to estimate human intention based on interaction forces, enhancing human-robot collaboration by dynamically adjusting the robot's behavior to align with the operator's intent. Nikolaidis et al. [Nikolaidis et al., 2015] developed a framework for learning human behavior from joint-action demonstrations using an inverse reinforcement learning algorithm and a Markov decision process, empowering a robot to formulate a robust policy for collaborative tasks with humans. In their experimental study, 36 human subjects engaged in a hand-finishing task, where their objective was to refinish the surface of a box held by an industrial robot. Simultaneously, the robot's role was to position the box according to human preferences. The findings indicated a higher consensus among participants regarding the robot's ability to anticipate their actions when utilizing the framework proposed by the authors, as opposed to manually annotating robot actions. Whitsell and Artemiadis [Whitsell and Artemiadis, 2017] presented a controller that allows humans to take leadership on desired axes while manipulating an object with a robot, incorporating force and torque data into a reinforcement learning algorithm for predicting future rewards. Ge et al. [Ge et al., 2011] utilized force, velocity, and position data at the interaction point between a robot arm and the human upper limb, feeding this information into an ANN model to estimate human motion intention, defined as the desired upper limb trajectory. This approach aligns with the study by Li and Ge [Li and Ge, 2014], where neural networks were used to estimate human motion intention, enhancing collaboration efficiency in scenarios with unpredictable human intentions. Guler et al. [Guler et al., 2022] implemented an ANN classifier to detect sub-tasks intended by the human operator during a collaborative drilling task, dynamically adjusting interaction controller parameters based on the detected sub-task to enhance task efficiency. Niaz et al. [Niaz et al., 2024] expanded upon this research by incorporating a "motion estimator" to anticipate the contact phase in advance, thereby facilitating smoother adjustments to controller parameters. Thobbi et al. [Thobbi et al., 2011] presented a framework for dynamic role adaptation in collaborative tasks, enhancing the flexibility and intuitiveness of human-robot interaction. This framework mainly consists of reactive and proactive controllers. The reactive controller generates a behavior for the robot based on the current state of the environment using a discrete Q-learning algorithm. In contrast, the proactive controller predicts human motion in the future time step, thereby determining the robot's proactive action. Lu et al. [Lu et al., 2020] employed a Long Short-Term Memory (LSTM) model to estimate human motion intention, focusing on desired trajectories in a human-robot collaborative task. Ly et al. [Ly et al., 2021] trained a Deep Q-Network to estimate human intentions in reaching pre-learned motion trajectories, providing adaptive haptic guidance on a robotic sorting task. Chien et al. [Chien et al., 2021] used a fuzzy radial basis function impedance compensator alongside an ANN model to compute hand compensation force, assisting the robot in following an intended trajectory. Wang et al. [Wang et al., 2018] addressed human intention estimation in hand-over tasks, utilizing inertial measurement unit (IMU) and electromyography (EMG) sensors for arm motion and muscle activity measurements. Their approach involved the extreme learning machine (ELM) algorithm for predicting human hand-over intention. Sirintuna et al. [Sirintuna et al., 2020b] utilized EMG signals to detect human intended movement directions by employing an ANN model. This allowed the admittance controller to constrain the robot's movements to those directions, resulting in reduced motion errors during collaborative positioning tasks.

2.5 Dyadic Behaviors in pHRI

The earlier studies discussed above, utilizing RB or ML approaches, have primarily focused on human behavior alone in detecting mostly motion intention to make the robot comply with these behaviors. In our earlier studies [Madan et al., 2015, Al-Saadi et al., 2021, Kucukyilmaz and Issak, 2020], we defined and classified dyadic interaction behaviors emerging from human partners' agreement or disagreement during collaborative tasks. Similarly, Cacace et al. [Cacace et al., 2018] explored dyadic behaviors, categorizing them into four different classes, including coinciding and opposite behaviors similar to harmonious and conflicting. These studies were effective in demonstrating the effectiveness of ML models and haptic features for the classification of dyadic interaction patterns in real-time collaboration.

2.6 Human Subjective Experience in pHRI

Studying dyadic behaviors in collaborative tasks involving both harmonious and conflicting interactions not only elucidates how mutual adaptation and shared mental models contribute to task performance and efficiency but also provides insights into the subjective and personal experiences of collaboration, a topic that receives less attention in pHRI. Human subjective experience plays an important role in pHRI by influencing user acceptance, trust, and collaboration with robots. These insights guide human-centered design, enhance usability, and contribute to the development of more comfortable, and user-friendly robotic interactions. According to Hoffman and Breazeal [Hoffman and Breazeal, 2010], anticipatory perceptual simulations in robots, which align with human cognitive expectations, significantly improve the efficiency and fluency of human-robot teams, further underpinning the importance of user-centered approaches in the design of interactive robots. Additionally, research by Baraglia et al. [Baraglia et al., 2016] underscores the benefits of proactive robot assistance in enhancing team fluency and subjective satisfaction. Gombolay et al. [Gombolay et al., 2015] further explore the dynamics of decision-making authority in human-robot teams, finding that while autonomous robots can outperform humans in task allocation, the distribution of decision-making authority significantly impacts team efficiency and worker satisfaction. Moreover, Nikolaidis et al. [Nikolaidis et al., 2017] demonstrate that robot motion planning that emphasizes predictability and legibility not only enhances the clarity of robotic intentions but also significantly boosts collaboration fluency. Their work shows that well-planned, legible robot motions, which are easily interpretable by human partners, can substantially improve the coordination and efficiency of joint tasks. Kulić and Croft [Kulic and Croft, 2007] emphasized the importance of a robot's response to human emotions for enhancing interaction quality. Additionally, Hu et al. [Hu et al., 2022] underline the importance of considering individual differences, such as personality traits and demographics, in the design of adaptive pHRI systems. Together, these studies underscore the significance of understanding and integrating the subjective human experience into human-centered design for more effective and comfortable pHRI.

Chapter 3

METHODOLOGY

This study investigates conflict-driven dyadic interaction patterns within pHRI, particularly focusing on co-manipulation scenarios. Our scenario involves a human and a robot collaboratively guiding an object toward a set of target locations (Figure 1.1). Our methodology, hinges on accurately detecting dyadic interaction patterns using an ML model, specifically a Random Forest classifier, that relies on haptic features alone. We define three interaction patterns (WP, CD, and CP) to describe two distinct groups of interaction (harmonious versus conflicting):

1. **WH: Working in Harmony:** Partners concur on the target direction, facilitating harmonious object movement.

2. **CD: Conflict in Target Direction:** A conflict in movement direction arises as partners aim for disparate target locations.

3. **CP: Conflict in Parking Location:** A conflict in parking location emerges when one partner intends to halt the object's motion before or after the mutual target location.

In our approach (outlined in Figure 3.1), the robot assumes a passive role at the start of co-manipulation and is hand-guided by the human. It collects force data (magnitude and direction) and stores it in a buffer for 160 ms (20 samples at 0.008 s each), which is compatible with the average human reaction time [Woods et al., 2015], to estimate the intended direction of human motion for manipulating the object. For this purpose, we calculate the average of the absolute differences between the force vectors stored in the buffer. Essentially, we calculate how much the force vectors in the buffer deviate from each other on average. If this deviation is below a certain threshold, the robot considers the direction of the average force vector as the direction of the movement intended by the human. Upon establishing the direction of movement, the robot sets a target location within its workspace. This process consists of extrapolating the vector estimated for the direction of movement and intersecting it with the surface representing the workspace boundary of the robot [Al-Saadi et al., 2023]. The robot then formulates an Artificial Potential Field (APF) to compute a trajectory (see Section 3.1 for details), transitioning to a proactive role in guiding the object toward this target by working in harmony (WH) with the human. If the human attains a new target direction while the robot is still pursuing the initial target, a "Conflict in Target Direction" (CD) emerges. Detecting this via ML, the robot abandons its current direction and passively follows the human until a new target direction and location are formulated. If the human changes the parking location along the movement path (i.e. if the human intends to park before/after the initial target), a 'Conflict in Parking Location' (CP) occurs. The robot becomes a follower again but increases its admittance damping to reduce the jerky movements of the human during the transition and help the human with accurate parking of the manipulated object to the new target location. The adjustment of the damping is regulated by our control architecture, which is further discussed in Section 3.2.

In the following subsections, we first discuss how we generate the trajectory for the robot based on the APF approach and then the control architecture of our pHRI system. The details of the classification process are given in the next section (Section 4).

3.1 Trajectory Generation

The trajectory for the robot, during its proactive collaboration with the human partner (WH), is generated by employing an APF, as detailed in our earlier publication [Al-Saadi et al., 2023]. In the APF, the total potential function, denoted as $U(Q)$, where Q is the current pose of the manipulated object (equivalent to the end effector position of the robot) is composed of an attractive potential, $U_{Att}(Q)$, and summation of repulsive potentials, $\sum U_{\mathrm{Rep}}(Q)$. Given the absence of physical obstacles within our experimental environment, the term for the repulsive potential function is omitted. Nevertheless, it is important to note that the proposed approach remains adaptable in the presence of obstacles without necessitating significant alterations. In such scenarios, the human, equipped with environmental awareness, would navigate to circumvent obstacles, while the robot would adjust its actions in response to the identified conflicts. The force exerted by the robot in contributing

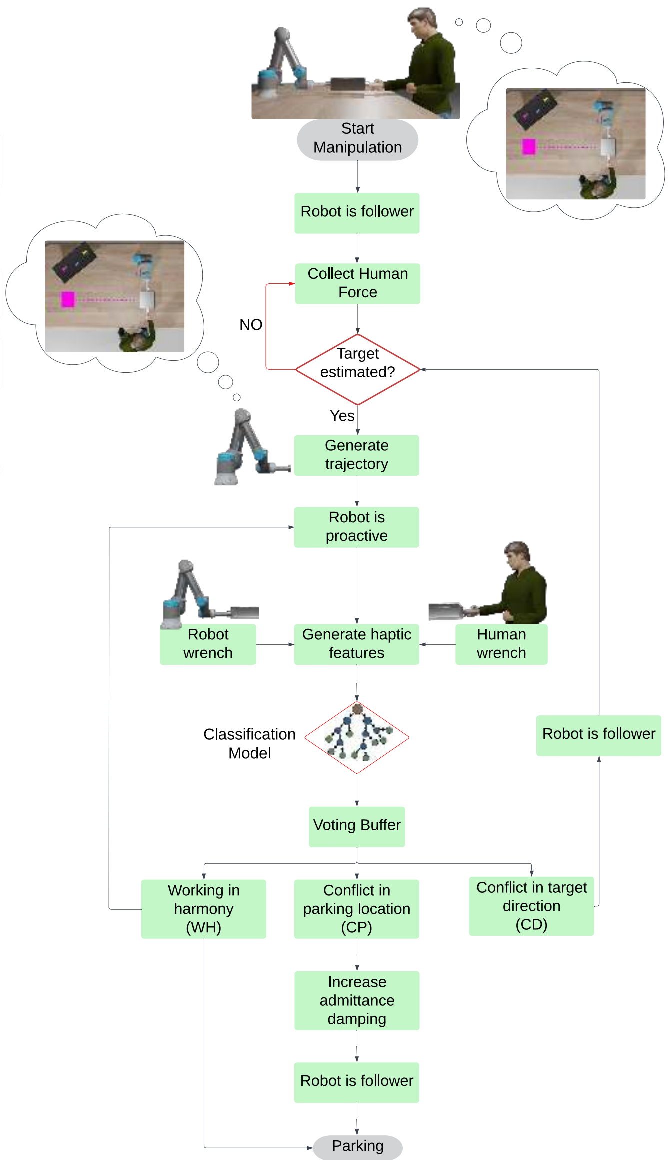

Figure 3.1: The flowchart of the proposed pHRI approach for co-manipulation of an object.

to the task is computed as the negative gradient of the total potential function, expressed as $F_{Att} = -\nabla U(Q) = \nabla U_{Att}$. This attractive force gradually decreases to zero as it gets closer to the target (Q_{Target}).

3.2 Control Architecture

The control architecture, as depicted in Figure 3.2, employs an admittance controller to regulate the physical interactions between the human and the robot. We utilize two decoupled admittance controllers to regulate the translational movements on the horizontal plane. Hence, the movements perpendicular to this plane and rotational movements are not allowed in our system.

The transfer function model of the admittance controller for each translational degree of freedom (dof) can be written as

$$Y(s) = \frac{V_{Ref}(s)}{F_T(s)} = \frac{1}{m_A s + b_A} = \frac{K_A}{\tau_A s + 1} \tag{3.1}$$

Here, m_A, b_A, $K_A = 1/b_A$ and $\tau_A = m_A/b_A$ represent the admittance mass, damping, gain, and time constant, respectively. $V_{Ref}(s)$ and $F_T(s)$ are the Laplace transformations for the reference velocity of the object and the total force applied to it. The values of the admittance mass and damping for each dof are $m_A = 3.25$ kg and $b_A = 60$ Ns/m, respectively [Hamad et al., 2021].

The robot estimates the target direction and location based on the force applied by the human to the object, F_H, after which the system generates a trajectory using the APF approach. This approach guides the robot towards the target with an attractive force F_{Att}. The total force F_T, a summation of F_H and F_{Att}, is then fed into the admittance controller, which outputs a reference velocity, V_{Ref}. The motion controller (PID) of the robot pushes the manipulated object with this reference velocity. The actual velocity achieved by the PID controller, V, is equivalent in magnitude to this reference velocity at frequencies below 5 Hz, with a negligible phase delay [Aydin et al., 2018].

At the beginning of co-manipulation, the robot is unaware of the target direction and location. During this phase, the ML model remains inactive, with the admittance controller responding solely to the human force input, F_H, since the robot does not contribute to the task (i.e. passive mode). As the robot becomes proactive ($F_{\text{Att}} \neq 0$), the ML model starts to predict the interaction patterns in real-time. It utilizes haptic features derived from the forces and torques exerted by the human and the robot to predict an interaction pattern at each time step of the control loop running at 125 Hz (Figure 3.2). The instantaneous predictions made by the ML model are stored in a voting buffer to enhance the accuracy of predictions by selecting the most frequently predicted interaction pattern in the buffer.

When the predicted pattern is harmonious (WH), the robot proactively engages in the task. However, in the case of a conflict (CD or CP), the robot resumes its follower role. During the transitions from WH to CD or CP, the robot's attractive force is gradually reduced to zero, smoothly transitioning from proactive mode to passive mode. In the case of CD, the target detection module is activated to estimate the new target direction and location, while in CP, the damping parameter of the admittance controller (i.e. parameter b_A in Equation (3.1)) is gradually increased to reduce the jerky behavior and aid the human in precise parking. Once the human moves the manipulated object sufficiently away from the current location defined by a threshold distance, the dyad is no longer in CP, the admittance damping is gradually reduced back to its nominal value, and the robot starts estimating a new target.

3.3 Hardware Configuration

The experimental framework employed in our research incorporates a UR5 collaborative robot, a plexiglass box-shaped object with dimensions 30 cm x 25 cm x 10 cm and a mass of 2.5 kg, a pair of force/torque (F/T) sensors (Mini45, ATI Inc.), and a computer display to offer visual feedback to participants (Figure 1.1). This configuration establishes a physical linkage between the human and the robot through the object being manipulated. The robot is rigidly connected to one side of the object using an F/T sensor, enabling the measurement of the robot-applied wrenches. On the opposite end, the human interacts with the object through an aluminum

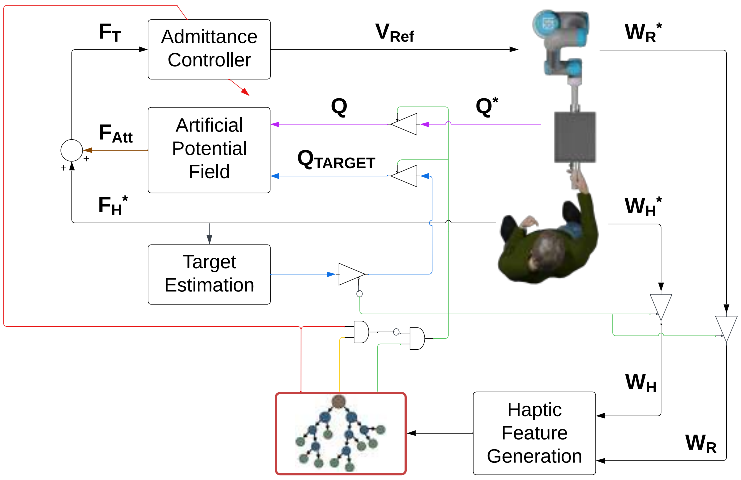

Figure 3.2: The control architecture utilized in our approach to regulate the harmonious and conflicting interactions between human and robot. The superscript asterisk signifies a variable directly measured by a sensor.

handle, with an attached F/T sensor capturing the wrenches applied by the human. Data acquisition is performed at a rate of 1 kHz utilizing an external DAQ card (USB-6343, National Instruments Inc.) connected to a personal computer.

Chapter 4

EVALUATION

This section presents a comprehensive evaluation of the proposed system, an analysis of the accuracy of the ML models in contrast to the RB, as well as discussing the results of two experimental studies: The training experiments focus on collecting essential data for training the ML models and comparing their classification accuracies through relatively simple manipulation scenarios. In contrast, the testing experiments rigorously compare the task performance under ML mode (based on the selected ML model) with three other interaction modes (*RB*, *Unyielding*, and *Passive*) through a controlled user study involving complex manipulation sequences.

4.1 Training Experiments

4.1.1 Training Scenarios

The training scenarios (see Figure 4.1) were crafted with the primary aim of gathering haptic data, which would be instrumental in training a classifier model capable of discerning between different interaction patterns, namely Working in Harmony (WH), Conflict in Target Direction (CD), and Conflict in Parking Location (CP). A total of 16 manipulation scenarios were devised, encapsulating a diverse array of interaction behaviors (Table 4.1). These training scenarios were not meant to be exhaustive but rather representative of a wide spectrum of potential interactions. In each scenario, the human and robot were tasked with collaboratively transporting an object from an initial location to one of several predetermined targets (A, B, C, D, E, F), as illustrated in Figure 4.1. The scenarios were strategically designed to induce both harmonious and conflicting patterns by programming the robot to follow a trajectory, which may not always coincide with the human partner's intentions.

Table 4.1: Training scenarios and the expected behaviors. The labels for the initial and final target locations correspond to the positions (A, B, C, D, E, F) shown in Figure 4.1

Training Scenario	Robot Target	Initial Human Target	Final Human Target	Expected Behavior
Tr-S1	B	B	B	WH
Tr-S2	E	E	E	WH
Tr-S3	B	E	E	CD
Tr-S4	E	B	B	CD
Tr-S5	B	E	A	WH, CP
Tr-S6	B	C	C	WH, CP
Tr-S7	E	D	D	WH, CP
Tr-S8	E	F	F	WH, CP
Tr-S9	B	B	F	WH, CD
Tr-S10	E	E	B	WH, CD
Tr-S11	E	B	D	CD, WH, CP
Tr-S12	E	B	F	CD, WH, CP
Tr-S13	B	E	A	CD, WH, CP
Tr-S14	B	E	C	CD, WH, CP
Tr-S15	E	B	E	CD, WH
Tr-S16	B	E	B	CD, WH

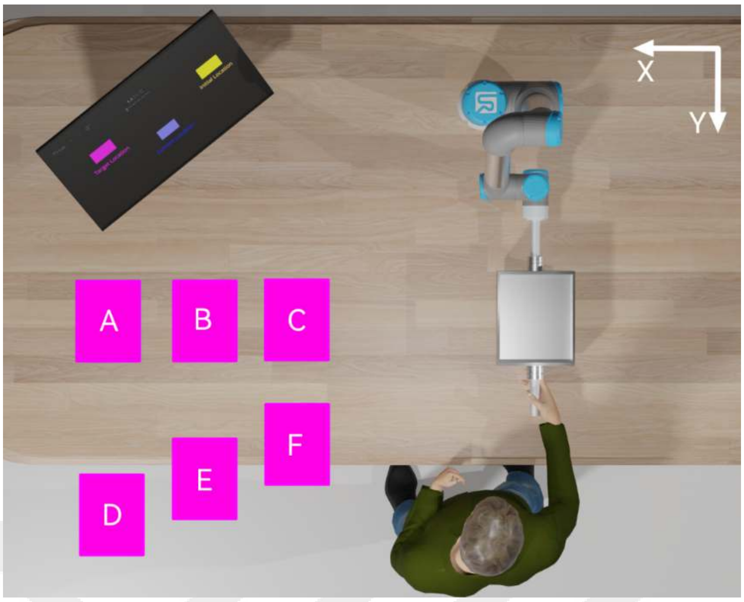

Figure 4.1: This illustration presents a bird's-eye view of a collaborative task between a human and a robot manipulating a rectangular box. The task involves moving the box on the horizontal plane (i.e. xy plane) from an initial position to one of the designated parking locations (A, B, C, D, E, and F). The details of the manipulation scenarios concerning these parking locations are given in Table 4.1. In executing these scenarios, visual guidance is provided to the participant through a computer monitor. The initial location, the intended target location, and the current location of the object were represented as 2D rectangles colored in yellow, pink, and blue on the monitor, respectively.

4.1.2 Participants and Protocol

Eight subjects (2 females and 6 males; average age: 26.3 ± 4.2 SD) participated in the training experiments. The protocol was designed such that participants were unaware of the robot's intended target. They were instructed to move the object toward their own chosen targets, without considering the robot's intentions. Each participant engaged in 32 trials, with every scenario being repeated twice. Hence, there were a total of 256 trials (8 participants x 32 trials/participant). To minimize bias, the order of scenarios was randomized for each session, yet it was consistent across all participants.

4.1.3 Haptic Features

Haptic features were derived from human and robot wrenches measured by the force sensors. It is important to note that using sensor data beyond just force/torque, such as object velocity, may further enhance classification accuracy, as demonstrated in our earlier work [Madan et al., 2015]. In that study, we showed that raw signals of force/torque are not sufficient to classify dyadic human-human interaction patterns with high accuracy, and incorporating object velocity enhances classification accuracy. In this study, we have employed a richer set of haptic features derived from force/torque data. These features, initially proposed by Noohi and Žefran [Noohi and Zefran, 2014] and extended by Al-Saadi et al. [Al-Saadi et al., 2021], form the basis for training our Random Forest classifier. Utilizing these rich haptic features results in higher classification accuracy compared to using raw force and torque signals alone. While we provide a brief overview here, comprehensive details can be found in [Al-Saadi et al., 2021].

The haptic features can be grouped into two: *force* and *torque*-related. Specifically, we utilize five force-related features: Individual Force Efficiencies (denoted as $M^F_{E_K}$), Team Force Efficiency (M^F_{TE}), Negotiation Force Efficiency (M^F_{NE}), and Similarity of Forces (M^F_S). Alongside these, we introduce five torque-related features, as detailed in our previous work [Al-Saadi et al., 2023]: Individual Torque Efficiencies ($M^\tau_{E_K}$), Team Torque Efficiency (M^τ_{TE}), Negotiation Torque Efficiency (M^τ_{NE}), and Similarity of Torques (M^τ_S).

In these symbols, the subscript K in $M^F_{E_K}$ and $M^\tau_{E_K}$ denotes the entity involved, which can be either a human (H) or a robot (R). The superscripts F and τ distinctly represent force and torque-related features, respectively. It is important to emphasize that all haptic metrics we discuss are normalized values, ranging between zero (0) and one (1), ensuring a standard scale for comparison and analysis.

Moreover, we categorize these features according to their contribution to the task, differentiating between *dyadic* and *individual* types. The Team Force Efficiency (M^F_{TE}), Negotiation Force Efficiency (M^F_{NE}), and Similarity of Forces (M^F_S), along with their torque counterparts, are the dyadic features. These metrics assess collaborative or interactive aspects, reflecting the efficiency and harmony in combined human-robot endeavors. In contrast, Individual Force Efficiencies ($M^F_{E_K}$) and Individual Torque Efficiencies ($M^\tau_{E_K}$) are categorized as the individual features. They primarily evaluate the performance or proficiency of singular entities, either human or robot, without direct consideration of their interaction dynamics. This distinction is pivotal for understanding and interpreting our data, as it sheds light on both collaborative and singular aspects of force and torque in human-robot interaction.

Building upon our previous work [Al-Saadi et al., 2023], we performed a decomposition of forces and torques in three principal movement planes (xy, xz, yz). This methodology resulted in 30 wrench-related features, with 10 wrench-related features per plane, which were then utilized as inputs for our classifier.

4.1.4 Data Annotation

Human and Robot Wrench Representations Our data contains human and robot wrench representations. The human wrench is derived from force and torque measurements, captured via a force sensor placed between the human's hand and the manipulated object. Similarly, the robot wrench was measured by a force sensor located between the object and the robot's end effector.

Annotation Procedure We animate the movement of the manipulated object in each trial using the recorded data for annotation (Figure 4.2), a crucial step implemented to facilitate accurate data labeling. This approach stands in contrast to direct labeling from raw data, which can often be overwhelming and more challenging to interpret. In the animations, the current location of the manipulated object is represented by a black rectangle, the robot's force vector is represented by a red arrow, its intended goal location by a dashed red rectangle, and the human's force vector by a blue arrow. These visual cues are designed to simplify the complexity of the data and aid in its interpretation. Working in Harmony (WH) is observed when both the robot's and human's force vectors are aligned and pointing toward a common goal, symbolizing a collaborative effort. In contrast, Conflict in Target

Direction (CD) is characterized by the human and robot force vectors diverging, signaling a discrepancy in the intended direction of movement. Finally, the interaction pattern is labeled as Conflict in Parking Location (CP) when the forces are along the same trajectory but have opposing directions, indicative of contention over the precise endpoint of the object's path.

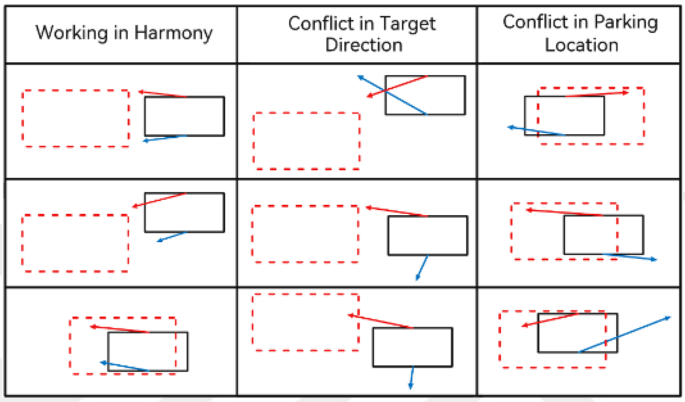

Figure 4.2: Data recorded during training experiments was animated for annotation. Each column in the figure shows a set of 3 exemplar screenshots captured from 3 different animated trials for each interaction pattern: WH, CD, and CP. The current location of the manipulated object is represented by a black rectangle, the robot's force vector is represented by a red arrow, its intended goal location is indicated by a dashed red rectangle, and the human's force vector is represented by a blue arrow.

The segments of the animated data were labeled by an expert (the first author of this paper) and a naive individual as WH, CD, or CP. The naive individual, unfamiliar with the experiment's specifics, was briefed on the training experiments before the labeling process. To ensure the naive individual fully grasps the process, he was initially asked to label a subset of 8 trials out of 256 trials under the guidance of the expert. Subsequently, both the expert and the naive individual independently labeled the remaining experimental trials.

The final labeling result was derived from a combined average of the labels given by both the expert and the naive individual. This method of averaging the two perspectives ensures a balanced and comprehensive interpretation of the data. Upon completion, any deviations between the expert's and the naive individual's labels were noted and analyzed. This analysis involves calculating the average deviation between their interpretations, thereby refining and concluding the labeling process. This systematic approach, leveraging both expert insights and fresh perspectives, enhances the reliability and accuracy of the labeling process.

4.2 Classifier Design and Implementation

In this subsection, we discuss our ML and RB models used for the classification of dyadic interaction patterns.

4.2.1 ML Models

We applied the following cross-validation methods to three types of ML models—ANN, Random Forest, and Support Vector Machines (SVM)—and tuned their hyperparameters to find the best configuration of each model.

- **K-Fold Cross-Validation:** The dataset was divided into the subsets of $K = 4, 5, 6, 8$. Each subset was used as a training set sequentially, with the remaining subsets forming the test set.

- **Subject-Wise Cross-Validation:** The dataset was divided into the subsets of $N = 4, 5, 6$ participants (recall that the total number of participants in the training experiments is 8). Each subset was used as a training set sequentially, with the remaining subsets forming the test set.

- **Trial-Wise Cross-Validation:** The dataset was divided into the subsets of $T = 22, 24, 26$ trials (recall that each participant undergoes a total of 32 trials in the training experiments). Each subset was used as a training set sequentially, with the remaining trials forming the test set.

Hence, there were a total of 10 (4+3+3) cross-validation runs.

Hyperparameter Search The following table summarizes the hyperparameter configurations explored for each model type:

Table 4.2: Hyperparameter Table for ML Models

Model	Hyperparameter
ANN	Number of neurons in each layer: (3,3), (3,8), (3,6,6), (3,16,8) (3,16,8,4), (16,8,8), (32,16,8), (32,16,16,8)
Random Forest	Number of decision trees: 10, 50 Maximum depth of each tree: 2, 5, 10 Minimum number of samples required to split a node: 2, 5
SVM	Regularization parameter: 0.1, 1, 10 Kernel: Polynomial, Radial Basis Function (RBF) Degree of the polynomial kernel: 3, 4, 5 Gamma: Scale, Auto

Model Performances We searched for the best set of hyperparameters that maximize each model's accuracy as measured by the cross-validation process (i.e. 10 cross-validation runs). Hence, for each hyperparameter configuration, the average classification accuracy of each ML model was calculated based on the cross-validation methods discussed above. Table 4.3 reports the accuracy results for each model with the best hyperparameter configuration. Based on these results, we selected Random Forest as our ML classifier.

Table 4.3: Averaged Cross-Validation Performances of ML Models for the Best Hyperparameter Configuration

Model	WH Accuracy	CD Accuracy	CP Accuracy	Total Accuracy
ANN	0.894	0.838	0.883	0.868
Random Forest	0.909	0.826	0.888	0.875
SVM	0.908	0.834	0.897	0.872

Feature Importance Once the ML model was selected as Random Forest, the significance of each feature in the model was evaluated (Figure 4.3). Given that the manipulation experiments involved object translation without rotation, force-related features were more critical than torque-related ones as expected. Based on this analysis, we removed the torque-related features from our ML model's input set (i.e., the number of features is reduced from 30 to 15). Additionally, the importance of force-related features alone in different planes (xy, yz, xz) revealed that the features defined for xy plane are more important than those in the other planes, aligning with the nature of the experiments (i.e. the object movements were in the xy plane). It was also observed that the individual features were of lesser importance than the dyadic features.

4.2.2 RB Model

As a baseline comparison with the proposed ML model, we developed an RB model to classify the interaction patterns (Figure 4.4). Our RB model relies on rules derived from the distribution of haptic features. However, the task of developing rules by inspecting the distribution of all 30 haptic features proved to be highly challenging. Based on the feature importance analysis given above, we ignored the torque-related features and also focused on the force-related features defined for the xy plane only. As a result, we have reduced the features whose distribution we inspect to derive classification rules to 5.

In our approach, the RB model first differentiates if the interaction is harmonious or conflicting. A harmonious interaction is immediately classified as WH (Working in Harmony). In the case of conflicting interaction, further classification into CD (Conflict in Target Direction) or CP (Conflict in Parking Location) is necessary.

The formulation of classification rules for the RB model was a tiring process, involving careful analysis of histograms of 5 different force-related features derived from the training data. This process was aimed at establishing thresholds to optimize the model's predictive accuracy, minimizing the inclusion of unwanted classes. An expert, with a deep understanding of interaction patterns and potential conflicts,

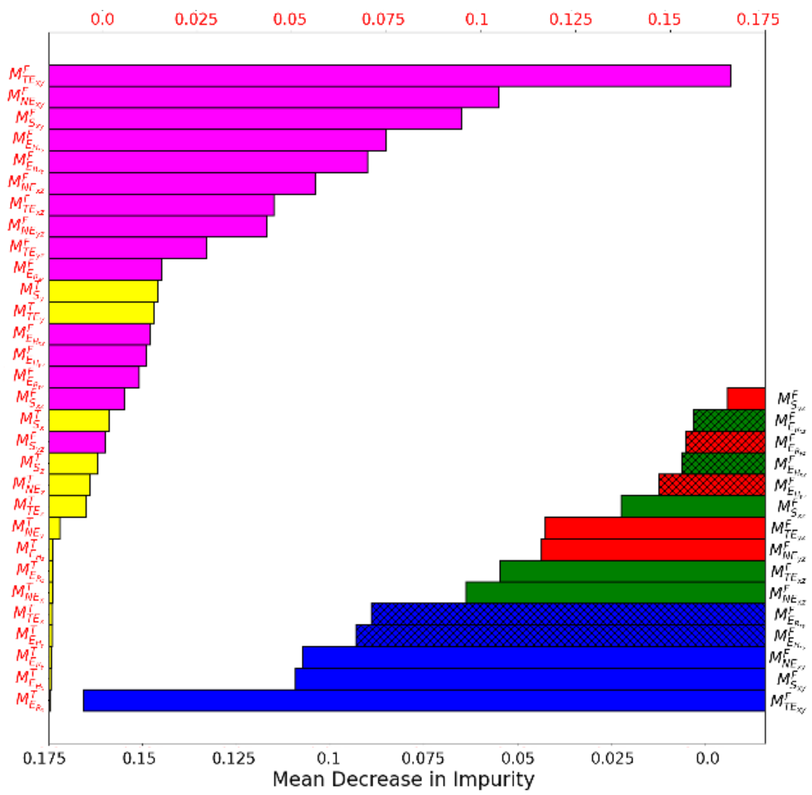

Figure 4.3: Bars on the left: Ranking of torque (yellow) and force features (purple) together based on their importance (i.e. mean decrease in impurity) in ML classification. Bars on the right: Ranking of force features alone for different coordinate planes based on their importance (i.e. mean decrease in impurity) in ML classification: xy-plane (blue), xz-plane (green), and yz-plane (red). Solid and hatched bars represent the dyadic and individual force features, respectively.

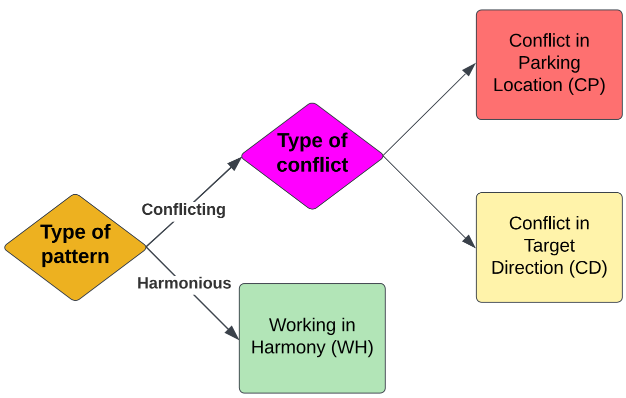

Figure 4.4: The flowchart for the RB model begins by determining whether the interaction pattern is harmonious or conflicting and then identifies the specific type of conflict.

played a pivotal role in crafting these rules.

To illustrate how these rules were constructed, let's consider an example involving the interaction pattern of WH. As depicted in Figure 4.5, the histogram for Negotiation Force Efficiency on the xy plane across different interaction patterns (WH, CD, and CP) served as a basis for the development of a rule used for differentiating if the interaction is harmonious or conflicting. If the Negotiation Force Efficiency on the xy plane exceeds the threshold value of 0.90, the interaction is most likely WH, with a possibility of being CD. To improve the accuracy of prediction, we incorporate another feature – Team Force Efficiency, as shown in the second column of the same figure. Setting a threshold value of 0.95 for Team Force Efficiency allows us to effectively filter out most CD cases. Hence, this two-step rule significantly enhances the accuracy of the WH classification.

These carefully crafted rules, combining multiple features and their respective thresholds, enable the RB model to classify 3 different interaction patterns successfully up to a certain degree when they are applied to the training data.

4.3 Performance Comparison of ML and RB Models

This evaluation is presented through confusion matrices, which summarize the results by comparing the actual and predicted classifications. They offer a clear visual and numerical representation of each model's predictive accuracy and areas where they might struggle.

ML Model Figure 4.6a presents the confusion matrix for the Random Forest classifier. The classification results reported in this figure are based on 6-fold subject-wise cross-validation with 8 participants. The high values at the diagonal indicate that the ML model correctly classifies all three interaction patterns, with particularly high accuracy for WH interactions.

RB Model The RB model achieves a lower accuracy than the ML model (Figure 4.6b). In particular, the RB model exhibits a high degree of confusion between

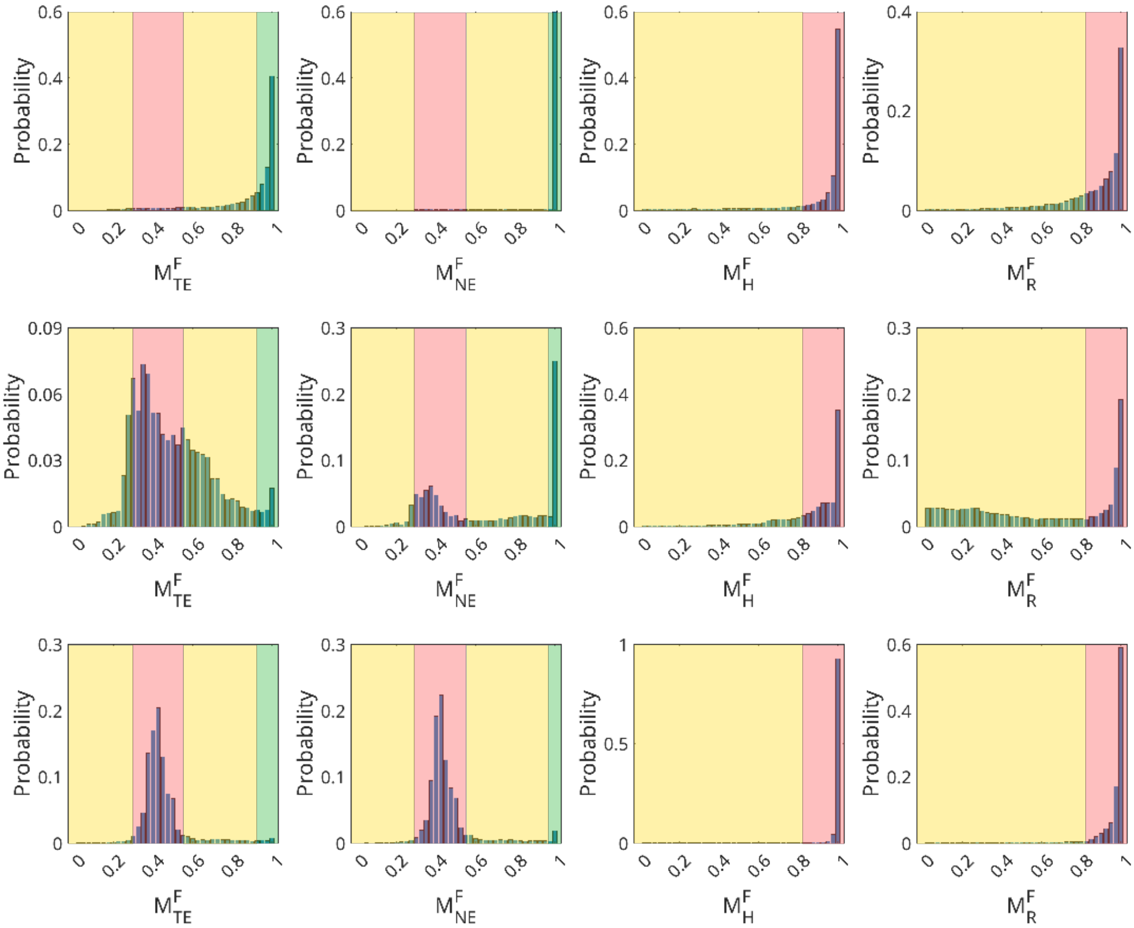

Figure 4.5: Histograms of the team force efficiency (M^F_{TE}), negotiation force efficiency (M^F_{NE}), human force efficiency ($M^F_{E_H}$), and robot force efficiency ($M^F_{E_R}$) for the xy-plane, arranged in columns from left to right. The first, second, and third rows show the metrics for WH, CD, and CP, respectively. The shaded regions, distinguished by green, yellow, and red hues, delineate the ranges of values employed to determine the interaction patterns of WH, CD, and CP, respectively.

CD and CP classes, suggesting a challenge in differentiating between these two conflict types.

4.4 *Testing Experiments*

4.4.1 Interaction Modes

The testing experiments employed a within-subjects design controlled user study, aimed at evaluating the robustness of the classifiers (ML and RB) versus the unyielding and passive robot behaviors in a more complex and dynamic interaction environment, bringing the evaluation one step closer to real-world settings. 20 participants (9 females, 11 males), who were not involved in the training experiments took part in the testing phase. The average age of these participants was 24.9 years (SD: $\pm$3.2 years).

Four interaction modes were controlled as independent variables in the study:

- *ML* mode utilized the APF with the ML classifier for conflict resolution.
- *RB* mode utilized the APF with the RB classifier for conflict resolution.
- *Unyielding* mode utilized the APF with no conflict resolution.
- *Passive* mode utilized the traditional leader-follower dynamic with the robot in a passive following role.

4.4.2 Testing Scenarios

These 4 interaction modes were interwoven into 5 distinct scenarios (Table 4.4), each designed to include a mixture of interaction patterns, arranged in continuous, back-to-back 4 sub-tasks to enrich the interaction complexity. A trial was considered complete when the object was successfully transported to and parked at all target locations, with the participant waiting for 3 seconds in the parking zone to confirm completion. This criterion ensured a consistent endpoint for each trial while allowing for the measurement of the classifiers' performance in sustained interaction sessions. Figure 4.7a shows all the manipulation locations used in the testing scenarios listed in Table 4.4.

The testing scenarios were designed to reflect the dynamic nature of human-robot interaction and to test the adaptability of our classifiers in a scenario where the target location could change during the task. Figure 4.7b exemplifies one such scenario (Ts-S2 from Table 4.4), graphically delineating the sequence of 4 sub-tasks that compose a single, complex interaction session. For example, in the first sub-task of this scenario (first row in Figure 4.7b), the robot and the human move

Table 4.4: Testing scenarios and the expected behaviors

Testing Scenario	Sub-Task	Starting Location	Initial Human Target	Intermediate Human Target	Final Human Target	Expected Behavior
Ts-S1	1	C_1	A_1	–	A	WH, CP
	2	A	C_1	–	C	WH, CP
	3	C	A_1	–	B_1	WH, CD
	4	B_1	D_1	–	C_1	WH, CD
Ts-S2	1	C_1	A_1	–	A	WH, CP
	2	A	C_1	–	D_1	WH, CD
	3	D_1	B_1	–	B_1	WH
	4	B_1	D_1	C_1	M	WH, CD, CP
Ts-S3	1	C_1	A_1	–	A_1	WH
	2	A_1	C_1	–	C_1	WH
	3	C_1	A_1	B_1	L	WH, CD, CP
	4	L	D_1	–	N	WH, CP
Ts-S4	1	C_1	A_1	–	A	WH, CP
	2	A	D_1	–	N	WH, CP
	3	N	B_1	–	B_1	WH
	4	B_1	D_1	C_1	M	WH, CD, CP
Ts-S5	1	C_1	A_1	–	B_1	WH, CD
	2	B_1	D_1	–	D	WH, CP
	3	D	A_1	–	A_1	WH
	4	A_1	C_1	–	C	WH, CP

toward the initial target (A_1). As they approach within a 10 cm range, the initial target disappears from the GUI, and the final target location (A) becomes visible —designing a sequence that incorporates both the 'Working in Harmony' (WH) and 'Conflict in Parking Location' (CP) interaction patterns. On the other hand, the last sub-task (fourth row in Figure 4.7b) introduces a more complex sequence: the robot and human initially move towards the first (initial) target (D_1). When they come within 30 cm of this target, it vanishes from the GUI, and a second (intermediate) target (C_1) appears. As the object nears this second target by 10 cm, the second target also disappears from the GUI, and the final target (M) appears. This sub-task was thus structured to induce a 'Working in Harmony' (WH) pattern, followed by a 'Conflict in Target Direction' (CD) when the first target shifts, and concluding with a 'Conflict in Parking Location' (CP) as they approach the final parking location.

4.4.3 Experimental Sessions

Each participant performed 10 trials (5 testing scenarios displayed twice) under each interaction mode as detailed in Section (4.4.1). These modes were displayed as Mode A, Mode B, Mode C, and Mode D to the participants on the computer monitor during the experiments to eliminate any bias due to naming. The trials were displayed to the participants in 4 separate blocks (each block represents one mode of interaction) and the blocks were randomized across the participants using a Latin squares design. This helps control for order effects or biases that might arise if the blocks were presented in a fixed order. To maintain a high level of concentration and reduce cognitive load, short breaks of two minutes were interspersed between the blocks for the participants.

4.4.4 Subjective Evaluation

After completing all the trials, participants revisited each mode to perform two additional trials. These trials served a dual purpose: to reinforce the participants' understanding of each mode and to provide a fresh context for informing their responses to the subsequent questionnaire. This session was crucial in assisting participants to remember the modes and discern the subtle differences among them, thereby enabling them to provide informed feedback.

The questionnaire was designed to encompass a broad spectrum of subjective experiences and included six questions of the NASA Task Load Index (TLX), measuring Mental Demand, Physical Demand, Temporal Demand, Performance, Effort, and Frustration. Beyond these workload-related questions, the questionnaire included 13 additional metrics to explore concepts crucial to human-robot interaction: Comfort, Trust, Enjoyment, Safety, Reliability, Responsiveness, Proactivity, Level of Control, Fluency, Robotic Assistance, Ease of Use, Perceived Usefulness, and Overall Satisfaction. Each of these additional metrics was probed with two questions—one phrased positively and the other negatively—to minimize response bias. The responses to all questions were measured on a 7-point Likert scale. For the case of 13 additional metrics, the responses were averaged after reversing the scores of negatively phrased questions. By incorporating positive and negative phrases for each variable on both task load and broader experiential factors, the questionnaire was able to capture a multi-faceted view of participant responses. The questionnaire responses provide detailed insights into the human aspect of human-robot interaction, which is as critical as any technical measure of system performance.

4.5 Statistical Analysis

The quantitative data were analyzed using a one-way repeated measures ANOVA to assess the impact of different interaction modes on the performance metrics. Mauchly's test was conducted to check if the assumption of sphericity was violated. If so, the degrees of freedom were corrected using Huynh-Feldt's estimates of sphericity. Finally, post hoc analysis was performed using the Tukey HSD test to determine significant differences between the interaction modes.

For the questionnaire data, due to the ordinal nature of the responses, a non-parametric Friedman test was conducted to assess the differences in the interaction modes across the subjective metrics. For post hoc analysis, the Tukey-Kramer method, adapted for non-parametric data, was used.

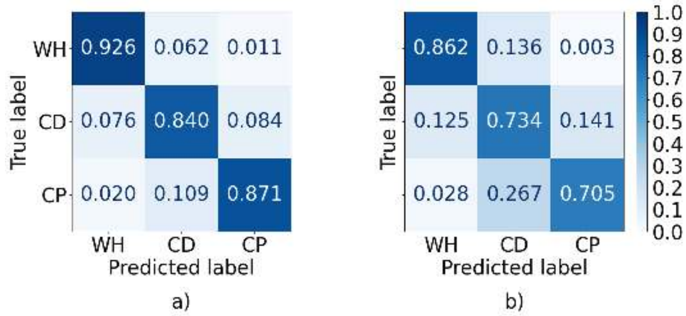

Figure 4.6: Confusion matrices of the ML (a) and RB (b) models for the training experiments.

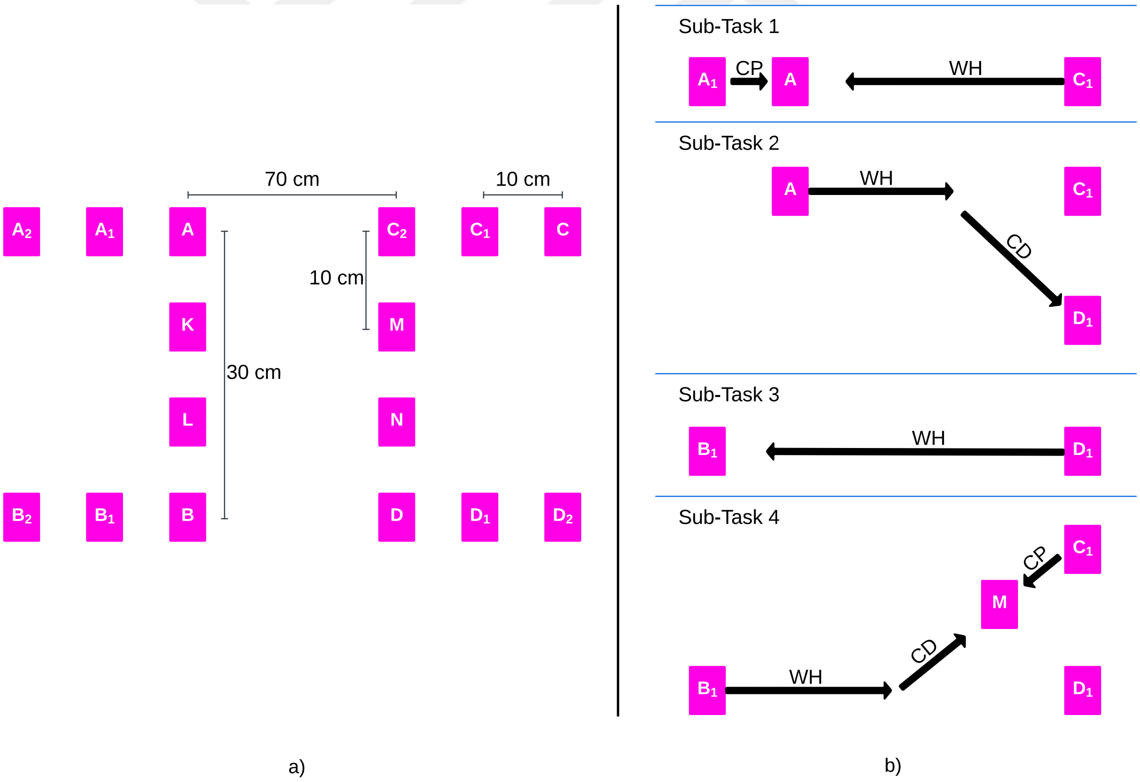

Figure 4.7: a) The manipulation locations used in the testing scenarios, with corresponding details provided in Table 4.4, b) An example of a testing scenario: Ts-S2 from Table 4.4. Each row represents the expected behavior in each sub-task of the scenario and the arrows show the expected direction of movement.

In all statistical analyses, star notation was used to indicate levels of statistical significance: one star (*), two stars (**), and three stars (***) denote $p < 0.05$, $p < 0.01$, and $p < 0.001$, respectively.

Chapter 5

RESULTS

This section presents results from the testing experiments and discusses their implications.

5.1 *Task Performance*

In evaluating the efficiency and effectiveness of human-robot interaction during task execution, several performance metrics were considered. These metrics provide insight into the task operation, the physical demands on the human operator, the efficiency of the task execution, and the precision and control of the object manipulation.

- **Average Force Applied by the Human (F_H^{AVE}):** This metric quantifies the mean force exerted by the human participant throughout the task, reflecting the physical effort required to achieve the objectives.

- **Average Object Velocity (V^{AVE}):** It measures the mean speed at which the object is moved from the start to the endpoint, indicating the pace of the task completion.

- **Average Power Consumed by the Human (P_H^{AVE}):** Representing the rate at which work is done by the human operator, this metric is calculated as the product of force and velocity, averaged over the duration of the task.

- **Task Completion Time (TCT):** The total time taken from the initiation to the successful completion of the task.

- **Average Settling Time**: The time required for the object to come to rest within a predefined area around the target, indicative of the control precision in the final task phase.

- **Average Number of Overshoots**: Counts how often the object passes beyond the target area before coming to rest, providing insight into the control and coordination of the movement.

- **Average Rise Time**: The duration from the start of the task until the object reaches its peak velocity, which reflects the responsiveness of the system to the human input.

- **Absolute Error in Parking**: The average of the maximum absolute difference between the final position of the object and the target location upon task completion, assessing the accuracy of the parking.

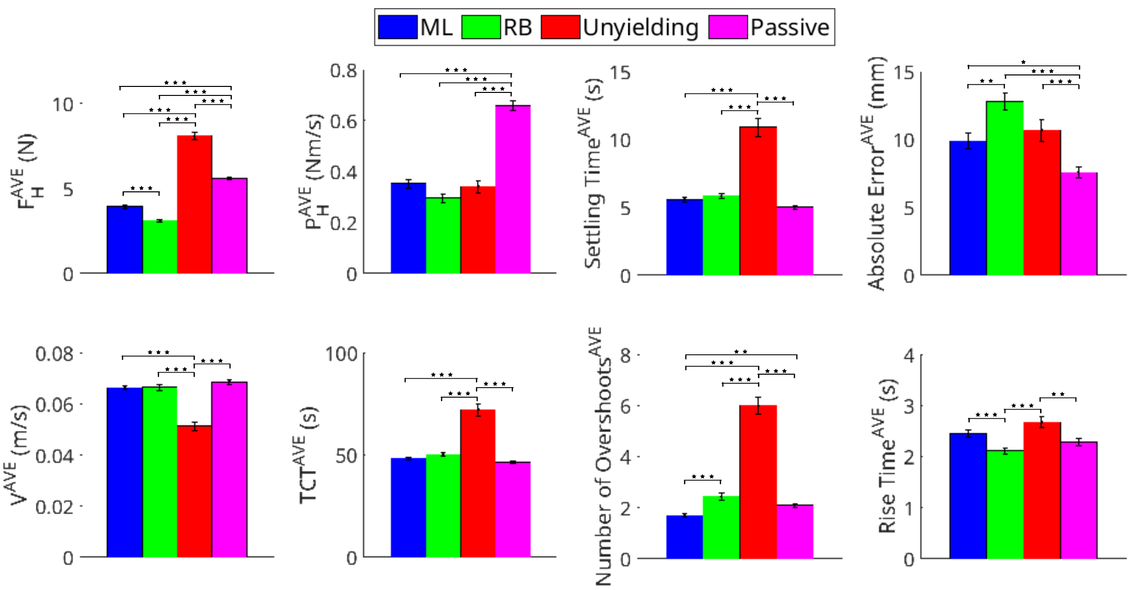

Figure 5.1: Bar plots display performance metrics for the interaction modes. The error bars indicate the standard errors of the means, while horizontal brackets with stars above them denote statistically significant differences, with one star (*), two stars (**), and three stars (***) indicating $p < 0.05$, $p < 0.01$, and $p < 0.001$, respectively.

Figure 5.1 presents the mean performance metrics for the interaction modes, computed over the data from 20 participants. An ANOVA revealed a significant effect of interaction mode on the average force applied by the human, F(3, 57) = 65.40, $p < 0.001$. Post hoc analysis showed that the *Unyielding* mode required the highest human force (M = 8.11 N, SE = 0.22) with $p < 0.001$ for all pairwise comparisons, signifying its status as the most force-demanding interaction strategy among the four modes. The *Passive* mode (M = 5.58 N, SE = 0.07) resulted in a significantly higher force than the *ML* mode (M = 3.93 N, SE = 0.10) with $p < 0.001$, while *RB* mode was characterized by the lowest force exertion by the participants (M = 3.13 N, SE = 0.08) with $p < 0.001$ for all pairwise comparisons.

An ANOVA indicated a significant effect of interaction mode on the average object velocity, F(3, 57) = 83.32, $p < 0.001$. Post hoc tests revealed that object velocity under the *Unyielding* mode (M = 0.05 m/s, SE = 1.6e-03) was significantly lower than those of the *ML* (M = 0.06 m/s, SE = 7.65e-04), *RB* (M = 0.06 m/s, SE = 9.89e-04), and *Passive* (M = 0.07 m/s, SE = 9.48e-04) modes, with $p < 0.001$. This indicates a slower task execution pace under the *Unyielding* mode compared to the other modes.

An ANOVA indicated a significant effect of interaction mode on the average power consumed by the human, F(3, 57) = 83.17, $p < 0.001$. Post hoc tests revealed that the *Passive* mode demanded the highest average power (M = 0.66 Nm/s, SE = 0.02) compared to the *ML* (M = 0.35 Nm/s, SE = 0.01), *RB* (M = 0.29 Nm/s, SE = 0.02), and *Unyielding* (M = 0.34 Nm/s, SE = 0.02) modes, all with statistical significance at $p < 0.001$. In our approach, we calculate the power as the product of human force and velocity of the object although there are more explicit methods in the literature for estimating human effort based on EMG measurements [Peternel et al., 2018].

An ANOVA revealed a significant effect of interaction mode on the task completion time, F(3, 57) = 88.56, $p < 0.001$. Post hoc analyses demonstrated that the *Unyielding* mode required the longest time to complete the task (M = 74.53 s, SE = 1.59), indicating a more time-intensive interaction for the human operator, compared to the *ML* (M = 48.78 s, SE = 0.28), *RB* (M = 51.07 s, SE = 0.52), and *Passive* (M = 47.44 s, SE = 0.32) modes, all with statistical significance at $p < 0.001$. Similarly, a higher number of overshoots were observed under the *Unyielding* mode (M = 6.01, SE = 0.35) compared to the other modes ($p < 0.001$), indicating a tendency to surpass the target area more frequently before stabilizing. On the other hand, *RB* mode had the highest absolute error in parking (M = 12.79 mm, SE = 0.64) although the difference from the *Unyielding* mode (M = 10.67 s, SE = 0.83) was not statistically significant ($p = 0.08$). *Passive* mode led to the lowest error (M = 7.58 mm, SE = 0.41) although the difference from the *ML* mode (M = 9.88 mm, SE = 0.58) was not statistically significant ($p = 0.82$).

5.2 Subjective Evaluation

The subjective evaluation of the interaction modes, as obtained from the participant responses to a questionnaire, provided critical insights into the human perceptions of the implemented human-robot collaboration paradigms. The questionnaire covered a spectrum of dimensions, from cognitive and physical demands to emotional and perceptual experiences during the interaction with the robot. Figure 5.2 illustrates participant ratings across four interaction modes.

The analysis of participants' responses to the questionnaire reveals a consistent trend across various subjective metrics, highlighting the distinct characteristics of each co-manipulation mode. Table 5.1 summarises the result of the statistical analyses for the subjective metrics. Friedman's ANOVA analysis showed no significant differences across the interaction modes for Temporal Demand ($\chi^2(3) = 2.72$, $p = 0.436$) and Robotic Assistance ($\chi^2(3) = 4.71$, $p = 0.194$). However, there were significant differences across the interaction modes for all the remaining subjective metrics, with statistical significance at $p < 0.001$, except for Responsiveness ($p = 0.0012$).

Table 5.2 tabulates the pairwise comparisons of the subjective metrics between the interaction modes. The *Passive* mode consistently outperformed the *Unyielding* mode across all metrics. However, the *Passive* mode received a statistically lower rating than other modes in terms of Proactivity. Ratings for the *Passive* mode were

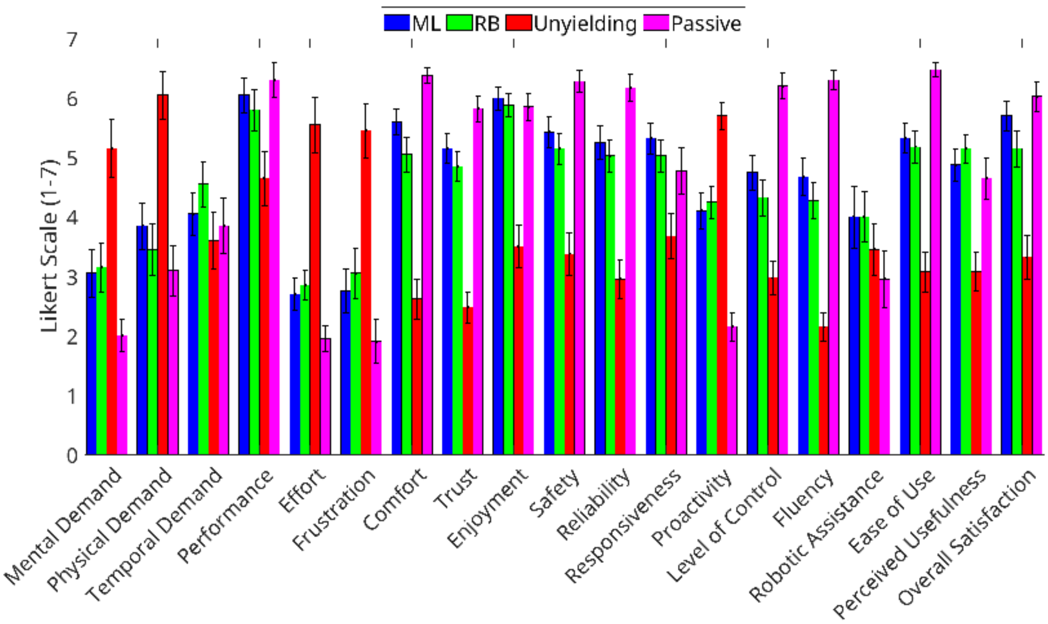

Figure 5.2: Following the experiments, a questionnaire was administered to the participants to assess their subjective opinions of the four different interaction modes. The error bars represent the standard errors of the means.

significantly higher than the *RB* mode in terms of Mental Demand, Comfort, Trust, Safety, Reliability, Level of Control, Fluency, and Ease of Use. On the other hand, participants rated the *Passive* mode significantly higher than the *ML* mode for Level of Control, Fluency, and Ease of Use metrics only.

Table 5.1: Friedman's ANOVA for Subjective Metrics

Subjective Metrics	Chi-square (χ^2)	p-value
Mental Demand	32.41	<0.001***
Physical Demand	29.40	<0.001***
Temporal Demand	2.72	0.4365
Performance	17.34	<0.001***
Effort	35.29	<0.001***
Frustration	31.19	<0.001***
Comfort	74.94	<0.001***
Trust	68.66	<0.001***
Enjoyment	50.32	<0.001***
Safety	52.09	<0.001***
Reliability	54.58	<0.001***
Responsiveness	15.90	0.0012**
Proactivity	61.38	<0.001***
Level of Control	46.44	<0.001***
Fluency	71.29	<0.001***
Robotic Assistance	4.71	0.1942
Ease of Use	63.44	<0.001***
Perceived Usefulness	27.92	<0.001***
Overall Satisfaction	37.42	<0.001***

p-values are indicated with stars to denote levels of statistical significance. One star (*) indicates $p < 0.05$, two stars (**) indicate $p < 0.01$, and three stars (***) indicate $p < 0.001$.

Table 5.2: The Pairwise Comparison of the Interaction Modes for the Subjective Metrics

Subjective Metrics	p-values					
	ML *RB*	*ML* *Unyielding*	*ML* *Passive*	*RB* *Unyielding*	*RB* *Passive*	*Unyielding* *Passive*
Mental Demand	0.8071	0.0011**	0.2453	0.0244*	0.0298*	<0.001***
Physical Demand	0.9881	<0.001***	0.7613	<0.001***	0.9146	<0.001***
Performance	0.9874	0.0149*	0.7520	0.0397*	0.5455	<0.001***
Effort	0.7071	<0.001***	0.6177	0.0044**	0.1013	<0.001***
Frustration	0.9847	0.0013**	0.2860	0.0047**	0.1441	<0.001***
Comfort	0.5593	<0.001***	0.2916	0.0018**	0.0115*	<0.001***
Trust	0.7056	<0.001***	0.3208	0.0018**	0.0279*	<0.001***
Enjoyment	0.9126	<0.001***	0.9675	<0.001***	0.9973	<0.001***
Safety	0.7917	<0.001***	0.1290	0.0066**	0.0103*	<0.001***
Reliability	0.7532	<0.001***	0.0573	0.0187*	0.0025**	<0.001***
Responsiveness	0.5392	0.0051**	0.3136	0.1979	0.9810	0.3833
Proactivity	0.9810	0.0375*	0.0051**	0.0998	0.0012**	<0.001***
Level of Control	0.8118	0.0549	0.0187*	0.3524	<0.001***	<0.001***
Fluency	0.3184	<0.001***	0.1365	0.0549	<0.001***	<0.001***
Ease of Use	0.9974	0.0016**	0.0275*	0.0033**	0.0153*	<0.001***
Perceived Usefulness	0.8081	0.0015**	0.9999	<0.001***	0.77	0.0019**
Overall Satisfaction	0.5422	<0.001***	0.9322	0.0655	0.2146	<0.001***

p-values are indicated with stars to denote levels of statistical significance. One star (*) indicates $p < 0.05$, two stars (**) indicate $p < 0.01$, and three stars (***) indicate $p < 0.001$.

Chapter 6

DISCUSSION

6.1 Task Performance

The task performance metrics provide a detailed insight into the operational characteristics of different interaction modes. A particularly interesting observation is the lower human force in *RB* mode compared to *ML* mode. A thorough investigation uncovered that *RB* mode's inability to accurately detect 'Conflict in Parking Location' (CP) pattern creates a misleading impression that humans apply less force under this mode. As illustrated by the confusion matrices in Figure 6.1, the RB model misclassifies CP as CD and occasionally as WH. In trials in which CP is correctly detected, the system would increase the damping to aid the human operator in parking the object with precision. This heightened damping leads to higher force exertion, but allows for more controlled and precise parking.

Conversely, as depicted in Figure 6.1, ML model demonstrates a higher accuracy in classifying interaction patterns (also observe that the voting buffer improves the classification accuracy). This capability allows the robot to adjust its behavior appropriately in *ML* mode, including increasing damping for CP cases, which in turn contributes to its superior performance in terms of lower overshoots and reduced absolute error in parking.

In contrast to *ML* and *RB* modes, which both implement conflict resolution strategies, *Unyielding* mode's performance reflects its approach to aiding the human only when both agents aim for the same target. Without a mechanism for conflict resolution, *Unyielding* mode leads to the highest force exerted by humans, suggesting a more strenuous interaction. This is also reflected in its prolonged task completion and settling times, indicating inefficiencies in its operational protocol that could be attributed to its lack of conflict resolution capability.

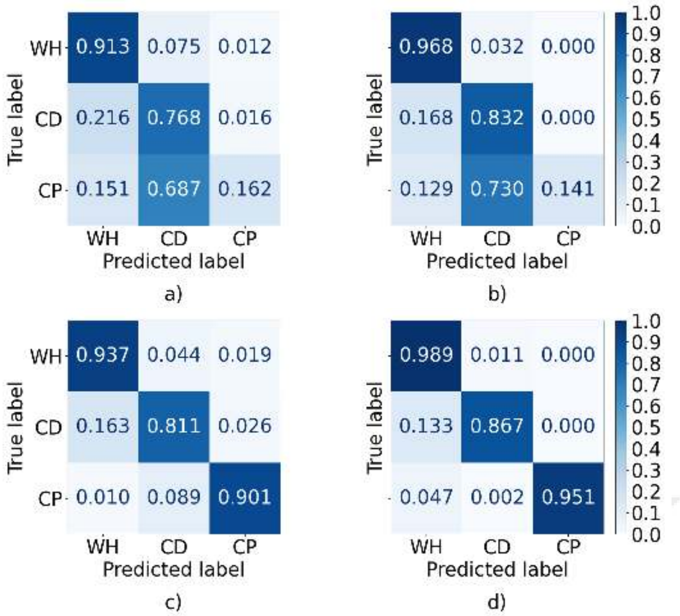

Figure 6.1: Confusion matrices for testing experiments: (a) RB model without voting buffer, (b) RB model with voting buffer, (c) ML model without voting buffer, and (d) ML model with voting buffer.

Passive mode, operating under a passive leader-follower dynamic, shows a distinctive pattern. Despite requiring substantial effort from the human operator, it does not necessarily achieve a faster task completion time. This highlights a potential inefficiency in the leader-follower mode where the robot's passive role could impose additional demands on the human operator without commensurate improvements in task performance [Mörtl et al., 2012].

The subpar task performances observed under *Unyielding* and *Passive* modes underscore the importance of active conflict resolution and proactive robot behavior in enhancing task efficiency and minimizing the physical burden on the human partner. The comparison of all modes suggests that a balanced approach involving both proactive behavior and effective conflict resolution, as seen in *ML* mode, tends to yield better overall task performance.

6.2 Subjective Evaluation

The results of the subjective evaluation indicate that the *Passive* mode was the most preferred by the participants in our co-manipulation scenarios, followed by the *ML* and *RB* modes, respectively. Conversely, the *Unyielding* mode was the least preferred mode of interaction. Here, we should emphasize that the *Passive* mode was rated higher than the *ML* mode in almost all metrics, but the differences were statistically significant for Reliability, Level of Control, and Ease of Use metrics only. On the other hand, the *Passive* mode was perceived as the least proactive among the four interaction modes.

The preference for the *Passive* mode among participants, despite its limitations in task performance, can be attributed to its Ease of Use, Level of Control, Fluency, Reliability, Safety, and Overall Satisfaction based on the subjective metrics used in the questionnaire. This preference underscores a strong inclination towards modes that afford greater human control and involve less demanding interactions, even at the expense of efficiency in task completion. Essentially, in *Passive* mode, the robot acts as a follower, mirroring human actions without introducing independent movements. This clear and predictable behavior is likely why the participants favored *Passive* mode. However, conducting a post-study interview would provide further insight into their choice.

Chapter 7

CONCLUSION

The comprehensive analysis of interaction modes in human-robot collaboration has provided valuable insights into the ideal design of these systems. Through a meticulous evaluation of task performance metrics and subsequent questionnaire analysis, this study has highlighted the delicate balance between task performance and subjective preference that is required for successful human-robot collaboration.

Our study reveals that while the *ML* mode demonstrates superior task performance and conflict resolution, it does not necessarily align perfectly with user preference. Conversely, the *Passive* mode, despite its limitations in task performance, is consistently preferred for its Ease of Use, Fluency, Level of Control, Reliability, Safety, and Overall Satisfaction. This preference indicates a strong inclination towards modes that give more control to humans and offer less demanding interaction, even if they are not the most efficient in task performance.

The *RB* mode, while sharing similarities with the *ML* mode, falls short in conflict resolution, particularly in the CP cases in our scenarios, affecting its overall efficiency and user preference. One can argue that better rules can be developed to detect CP, but as discussed earlier, this is a tedious and time-consuming process. This underscores the value of our ML approach in identifying dyadic interaction patterns in collaborative tasks. The *Unyielding* mode, with its absence of a conflict resolution mechanism, not only places the highest physical demands on the operator but also ranks lowest in user preference, emphasizing its impracticality in collaborative environments.

In conclusion, this study highlights the practicality and effectiveness of ML-based approaches over RB-based approaches in classifying interaction patterns during pHRI tasks. However, it underscores the importance of designing pHRI systems tailored not only for optimal task performance but also with due consideration for human needs and preferences regarding interaction modes.

Our current classification approach detects the interaction patterns at the current time step based on the past values of haptic features, and hence it is blind to the future. If, for example, the occurrence of CD or CP in the future is anticipated in advance, the force applied by the robot to the object can be gradually reduced to facilitate a smoother transition of the robot to the *Passive* mode. This approach has the potential to enhance not only classification accuracy, particularly for Conflict in Target Direction (CD) and Conflict in Parking Location (CP), but also to cultivate a perception of the robot as more accommodating, thus potentially influencing the user's subjective experience positively. An additional avenue for improvement involves enhancing the compliance of the APF approach with human intentions. In our current approach, the robot force is generated by APF solely based on the object's position. Nevertheless, integrating object velocity and acceleration into the APF model could enhance the adaptation of robot force, better aligning with and accommodating human intentions. Finally, our approach utilizes two force sensors (one on the robot side and one on the human side), which may not be practical due to the force sensor on the human side. Our future studies will focus on estimating human force using human arm kinematics and a musculoskeletal model of the human arm.

BIBLIOGRAPHY

[Al-Saadi et al., 2023] Al-Saadi, Z., Hamad, Y. M., Aydin, Y., Kucukyilmaz, A., and Basdogan, C. (2023). Resolving conflicts during human-robot co-manipulation. In *Proceedings of the 2023 ACM/IEEE International Conference on Human-Robot Interaction*, HRI '23, page 243–251, New York, NY, USA. Association for Computing Machinery.

[Al-Saadi et al., 2021] Al-Saadi, Z., Sirintuna, D., Kucukyilmaz, A., and Basdogan, C. (2021). A novel haptic feature set for the classification of interactive motor behaviors in collaborative object transfer. *IEEE Transactions on Haptics*, 14(2):384–395.

[Aydin et al., 2021] Aydin, Y., Sirintuna, D., and Basdogan, C. (2021). Towards collaborative drilling with a cobot using admittance controller. *Transactions of the Institute of Measurement and Control*, 43(8):1760–1773.

[Aydin et al., 2018] Aydin, Y., Tokatli, O., Patoglu, V., and Basdogan, C. (2018). Stable physical human-robot interaction using fractional order admittance control. *IEEE Transactions on Haptics*, 11(3):464–475.

[Aydin et al., 2020] Aydin, Y., Tokatli, O., Patoglu, V., and Basdogan, C. (2020). A computational multicriteria optimization approach to controller design for physical human-robot interaction. *IEEE Transactions on Robotics*, 36(6):1791–1804.

[Baraglia et al., 2016] Baraglia, J., Cakmak, M., Nagai, Y., Rao, R., and Asada, M. (2016). Initiative in robot assistance during collaborative task execution. In *2016 11th ACM/IEEE International Conference on Human-Robot Interaction (HRI)*, pages 67–74.

[Basdogan et al., 2000] Basdogan, C., Ho, C.-H., Srinivasan, M. A., and Slater, M. (2000). An experimental study on the role of touch in shared virtual environments. *ACM Transactions on Computer-Human Interaction (TOCHI)*, 7(4):443–460.

[Bussy et al., 2012] Bussy, A., Gergondet, P., Kheddar, A., Keith, F., and Crosnier, A. (2012). Proactive behavior of a humanoid robot in a haptic transportation task with a human partner. In *2012 IEEE RO-MAN: The 21st IEEE International Symposium on Robot and Human Interactive Communication*, pages 962–967.

[Cacace et al., 2018] Cacace, J., Finzi, A., Lippiello, V., et al. (2018). Shared admittance control for human-robot co-manipulation based on operator intention estimation. In *ICINCO (2)*, pages 71–80.

[Chien et al., 2021] Chien, S.-H., Wang, J.-H., and Cheng, M.-Y. (2021). Robotic assistance for physical human–robot interaction using a fuzzy rbf hand impedance compensator and a neural network based human motion intention estimator. *IEEE Access*, 9:126048–126057.

[Ge et al., 2011] Ge, S. S., Li, Y., and He, H. (2011). Neural-network-based human intention estimation for physical human-robot interaction. In *2011 8th International Conference on Ubiquitous Robots and Ambient Intelligence (URAI)*, pages 390–395.

[Gombolay et al., 2015] Gombolay, M. C., Gutierrez, R. A., Clarke, S. G., Sturla, G. F., and Shah, J. A. (2015). Decision-making authority, team efficiency and human worker satisfaction in mixed human—robot teams. *Auton. Robots*, 39(3):293–312.

[Guler et al., 2022] Guler, B., Niaz, P. P., Madani, A., Aydin, Y., and Basdogan, C. (2022). An adaptive admittance controller for collaborative drilling with a robot based on subtask classification via deep learning. *Mechatronics*, 86:102851.

[Hamad et al., 2021] Hamad, Y. M., Aydin, Y., and Basdogan, C. (2021). Adaptive human force scaling via admittance control for physical human-robot interaction. *IEEE Transactions on Haptics*, 14(4):750–761.

[Hoffman et al., 2024] Hoffman, G., Bhattacharjee, T., and Nikolaidis, S. (2024). Inferring human intent and predicting human action in human–robot collaboration. *Annual Review of Control, Robotics, and Autonomous Systems*, 7(1):null.

[Hoffman and Breazeal, 2010] Hoffman, G. and Breazeal, C. (2010). Effects of anticipatory perceptual simulation on practiced human-robot tasks. *Auton. Robots*, 28(4):403–423.

[Hu et al., 2022] Hu, Y., Abe, N., Benallegue, M., Yamanobe, N., Venture, G., and Yoshida, E. (2022). Toward active physical human–robot interaction: quantifying the human state during interactions. *IEEE Transactions on Human-Machine Systems*, 52(3):367–378.

[Kang et al., 2019] Kang, G., Oh, H. S., Seo, J. K., Kim, U., and Choi, H. R. (2019). Variable admittance control of robot manipulators based on human intention. *IEEE/ASME Transactions on Mechatronics*, 24(3):1023–1032.

[Khoramshahi and Billard, 2019] Khoramshahi, M. and Billard, A. (2019). A dynamical system approach to task-adaptation in physical human–robot interaction. *Auton Robot*, 43:927–946.

[Khoramshahi and Billard, 2020] Khoramshahi, M. and Billard, A. (2020). A dynamical system approach for detection and reaction to human guidance in physical human–robot interaction. *Auton Robot*, 44:1411–1429.

[Kucukyilmaz and Issak, 2020] Kucukyilmaz, A. and Issak, I. (2020). Online identification of interaction behaviors from haptic data during collaborative object transfer. *IEEE Robotics and Automation Letters*, 5(1):96–102.

[Kucukyilmaz et al., 2013] Kucukyilmaz, A., Sezgin, T. M., and Basdogan, C.

(2013). Intention recognition for dynamic role exchange in haptic collaboration. *IEEE Transactions on Haptics*, 6(1):58–68.

[Kulic and Croft, 2007] Kulic, D. and Croft, E. A. (2007). Affective state estimation for human–robot interaction. *IEEE Transactions on Robotics*, 23(5):991–1000.

[Lecours et al., 2012] Lecours, A., Mayer-St-Onge, B., and Gosselin, C. (2012). Variable admittance control of a four-degree-of-freedom intelligent assist device. In *2012 IEEE International Conference on Robotics and Automation*, pages 3903–3908.

[Li and Ge, 2014] Li, Y. and Ge, S. S. (2014). Human–robot collaboration based on motion intention estimation. *IEEE/ASME Transactions on Mechatronics*, 19(3):1007–1014.

[Losey et al., 2018] Losey, D. P., McDonald, C. G., Battaglia, E., and O'Malley, M. K. (2018). A review of intent detection, arbitration, and communication aspects of shared control for physical human–robot interaction. *Applied Mechanics Reviews*, 70(1):010804.

[Lu et al., 2020] Lu, W., Hu, Z., and Pan, J. (2020). Human-robot collaboration using variable admittance control and human intention prediction. In *2020 IEEE 16th International Conference on Automation Science and Engineering (CASE)*, pages 1116–1121.

[Ly et al., 2021] Ly, K. T., Poozhiyil, M., Pandya, H., Neumann, G., and Kucukyilmaz, A. (2021). Intent-aware predictive haptic guidance and its application to shared control teleoperation. In *2021 30th IEEE International Conference on Robot and Human Interactive Communication (RO-MAN)*, pages 565–572.

[Madan et al., 2015] Madan, C. E., Kucukyilmaz, A., Sezgin, T. M., and Basdogan, C. (2015). Recognition of haptic interaction patterns in dyadic joint object manipulation. *IEEE Transactions on Haptics*, 8(1):54–66.

[Madani et al., 2022] Madani, A., Niaz, P. P., Guler, B., Aydin, Y., and Basdogan, C. (2022). Robot-assisted drilling on curved surfaces with haptic guidance under adaptive admittance control. In *2022 IEEE/RSJ International Conference on Intelligent Robots and Systems (IROS)*, pages 3723–3730. IEEE.

[Mielke et al., 2024] Mielke, E., Townsend, E., Wingate, D., Salmon, J. L., and Killpack, M. D. (2024). Human-robot planar co-manipulation of extended objects: data-driven models and control from human-human dyads. *Frontiers in Neurorobotics*, 18:1291694.

[Mörtl et al., 2012] Mörtl, A., Lawitzky, M., Kucukyilmaz, A., Sezgin, M., Basdogan, C., and Hirche, S. (2012). The role of roles: Physical cooperation between humans and robots. *The International Journal of Robotics Research*, 31(13):1656–1674.

[Niaz et al., 2024] Niaz, P. P., Erzin, E., and Basdogan, C. (2024). Efficient and safe contact-rich phri via subtask detection and motion estimation using deep learning.

[Nikolaidis et al., 2017] Nikolaidis, S., Hsu, D., and Srinivasa, S. (2017). Human-robot mutual adaptation in collaborative tasks: Models and experiments. *The International Journal of Robotics Research*, 36(5-7):618–634. PMID: 32855581.

[Nikolaidis et al., 2015] Nikolaidis, S., Ramakrishnan, R., Gu, K., and Shah, J. (2015). Efficient model learning from joint-action demonstrations for human-robot collaborative tasks. In *2015 10th ACM/IEEE International Conference on Human-Robot Interaction (HRI)*, pages 189–196.

[Noohi and Zefran, 2014] Noohi, E. and Zefran, M. (2014). Quantitative measures of cooperation for a dyadic physical interaction task. In *2014 IEEE-RAS International Conference on Humanoid Robots*, pages 469–474.

[Oguz et al., 2010] Oguz, S. O., Kucukyilmaz, A., Sezgin, T. M., and Basdogan, C.

(2010). Haptic negotiation and role exchange for collaboration in virtual environments. In *2010 IEEE haptics symposium*, pages 371–378. IEEE.

[Oguz et al., 2012] Oguz, S. O., Kucukyilmaz, A., Sezgin, T. M., and Basdogan, C. (2012). Supporting negotiation behavior with haptics-enabled human-computer interfaces. *IEEE Transactions on Haptics*, 5(3):274–284.

[Peternel et al., 2018] Peternel, L., Tsagarakis, N., Caldwell, D., et al. (2018). Robot adaptation to human physical fatigue in human-robot co-manipulation. *Autonomous Robots*, 42(5):1011–1021.

[Sirintuna et al., 2020a] Sirintuna, D., Aydin, Y., Caldiran, O., Tokatli, O., Patoglu, V., and Basdogan, C. (2020a). A variable-fractional order admittance controller for phri. In *2020 IEEE International Conference on Robotics and Automation (ICRA)*, pages 10162–10168.

[Sirintuna et al., 2020b] Sirintuna, D., Ozdamar, I., Aydin, Y., and Basdogan, C. (2020b). Detecting human motion intention during phri using artificial neural networks trained by emg signals. In *2020 29th IEEE International Conference on Robot and Human Interactive Communication (RO-MAN)*, pages 1280–1287.

[Thobbi et al., 2011] Thobbi, A., Gu, Y., and Sheng, W. (2011). Using human motion estimation for human-robot cooperative manipulation. In *2011 IEEE/RSJ International Conference on Intelligent Robots and Systems*, pages 2873–2878.

[Townsend et al., 2017] Townsend, E. C., Mielke, E. A., Wingate, D., and Killpack, M. D. (2017). Estimating human intent for physical human-robot comanipulation. *CoRR*, abs/1705.10851.

[Wang et al., 2018] Wang, W., Li, R., Chen, Y., and Jia, Y. (2018). Human intention prediction in human-robot collaborative tasks. In *Companion of the 2018 ACM/IEEE International Conference on Human-Robot Interaction*, HRI '18, page 279–280, New York, NY, USA. Association for Computing Machinery.

[Whitsell and Artemiadis, 2017] Whitsell, B. and Artemiadis, P. (2017). Physical human-robot interaction (phri) in 6 dof with asymmetric cooperation. *IEEE Access*, 5:10834–10845.

[Wojtara et al., 2009] Wojtara, T., Uchihara, M., Murayama, H., Shimoda, S., Sakai, S., Fujimoto, H., and Kimura, H. (2009). Human–robot collaboration in precise positioning of a three-dimensional object. *Automatica*, 45(2):333–342.

[Woods et al., 2015] Woods, D. L., Wyma, J. M., Yund, E. W., Herron, T. J., and Reed, B. (2015). Factors influencing the latency of simple reaction time. *Frontiers in Human Neuroscience*, 9:131.